JOURNAL OF MATERIALS SCIENCE 11 (1976) 164–185

Review
Amorphous structures and their formation and stability

S. TAKAYAMA
Materials Research Center, Allied Chemical Corporation, Morristown, N.J., USA

The formation and stability of amorphous alloys are discussed in terms of the configurational entropy and in connection with the potential barrier, $\Delta\mu$. The structure analysis of amorphous alloys using Bernal's dense random packing model (D.R.P.) shows quite good agreement with the actual observations. These results indicate that some degree of short range order (~ 15 Å) exists in amorphous metallic alloys, which is slightly different from the arrangement expected in a liquid. The model still shows a continuous structure without the formation of internal boundaries between ordered regions such as is characteristic of polycrystals. Although the D.R.P. does not completely reflect the structure of amorphous alloys, it is still an attractive model in understanding the amorphous state. These subjects are reviewed in this article.

1. Introduction

The fact that an amorphous structure could exist in some materials has been known for some time. For example, we could easily find it in some natural silica glasses and polymers. Usually, the amorphous structure could be defined by the absence of long range order (similar to a liquid) in contrast to crystalline materials showing long range order with a repeating unit cell. This liquid-like structure could also be sustained in metals under special conditions. These facts have been known for more than three decades [1]. Such kinds of metals (or alloys) are called "amorphous metals (or alloys), liquid metals (or alloys)", non-crystalline metals (or alloys), glassy metals, Metglas, or metallic glasses. The alloys which are called amorphous are generally characterized by a diffuse halo X-ray diffraction pattern and show no contrast in transmission electron microscopy (TEM). That the atomic arrangement of these amorphous alloys, however, is not completely random, but maintains a greater degree of short range order than that in a liquid, was first pointed out by Dixmier *et al.* [2] in Ni–P amorphous alloys. Thereafter, analysis of the radial distribution function (R.D.F.) calculated from the reflected intensity measurements in X-ray diffraction has also shown the existence of short range order less than 15 Å in various amorphous alloys [3–8].

The investigation of amorphous metallic alloys started with electrolytic deposition [9], chemical (electroless) deposition [9–12] and evaporation deposition [13–15] (vapour deposition on cold substrates) and included the systems, Ni–S, Ni–B, Ni–P and Sn–Cu, and the elements Si, Bi and Ga. A large number of studies of the properties and structure in these alloys, have been conducted after the splat quenching method was developed by Klement *et al.* in the Au–Si systems [16]. Many interesting properties have been revealed by structural, electrical, thermodynamic and magnetic analysis (see review articles [17] and [18] of the splat-quenched alloys).

2. Quenching methods

Amorphous phases may be prepared not only by a supercooling method but also by other methods if the cooling rate is high enough to suppress the nucleation and growth of the crystallization from a liquid state [17]. Accordingly, it was predicted that a cooling rate of about 10^{6° C sec^{-1} would be required to reach this result [19]. For this purpose, several methods have been used. One of these is the "gun technique", developed by Duwez and

TABLE I Various splat quenching methods

Method	Cooling rate (°C sec^{-1})	Sample shape	Reference
Gun	10^6 to 10^8	Irregular thin film or powder (uniform thickness)	[20]
Piston and anvil	10^6 to 10^7	Irregular thin plates (rather uniform thickness)	[22]
Plasm-jet	~ 10^7	Irregular thin film (uniform thickness)	[24]
Torsion catapult	~ 10^6	Irregular thin plates (uniform thickness)	[26]
Drum quenching	~ 10^6	Regular uniform ribbon filaments (uniform thickness)	[27]
Roller quenching	~ 10^6	Regular thin plates (uniform thickness)	[28]

co-workers [20, 21], in which a globule of molten metal is acclerated to a high speed by high pressure helium gas, and fired at a cooled copper substrate. The other method is the "piston and anvil technique" developed by Pietrokoswky [22] where advantage is taken of the thermal conduction of metals. Drops of molten metal are squeezed flat between two rapidly moving cooled copper plates. This method was later combined with the gun technique, and called the "gun and piston-anvil technique" [23]. A plasmajet spray technique has also been used appreciably to obtain a fast quenching rate. In this technique a molten alloy in a plasma flame is splashed and quenched on a flat copper plate [24, 25]. The "torsion catapult technique" [26] where a molten alloy, forced by torsion, is catapulted against a cooled copper substrate yielding a somewhat continuous foil, is another way to satisfy this condition. Yet the shape and size of amorphous alloys produced by these methods are not adequate to conduct quantitative measurements on mechanical properties.

These limitations have been recently removed by a drum quenching technique developed by Pond and Maddin [27] and also by a roller quenching technique due to Chen and Miller [28]. The former is the method in which ribbon filaments of the amorphous alloys are made by quenching from the liquid state along the inside cylindrical surface of a rotating drum. The latter method is one in which uniform long samples are produced due to flattening out quenching of dropped alloys between two rotating wheels. These two technique offer not only the advantage of producing uniform shape and size of amorphous alloys, but also the possibility of mass producing the alloys (a most worthwhile contribution) [29]. A list of the various splat quenching methods is compiled in Table I.

3. Amorphous alloy systems

So far, a large number of amorphous alloys have been reported. These amorphous materials are summarized in Table II, excluding the oxide natural glasses and most of the chalcogenide glasses which are well known as amorphous semiconductors. In Table II, EV, CD, SQ, ED and P denote the abbreviations of vapour deposition, chemical deposition, splat quenching (or sputtering), electrolytic deposition, and plasmajet deposition, respectively. "Pure" means the amorphous materials are obtained even with the pure elements. Reference

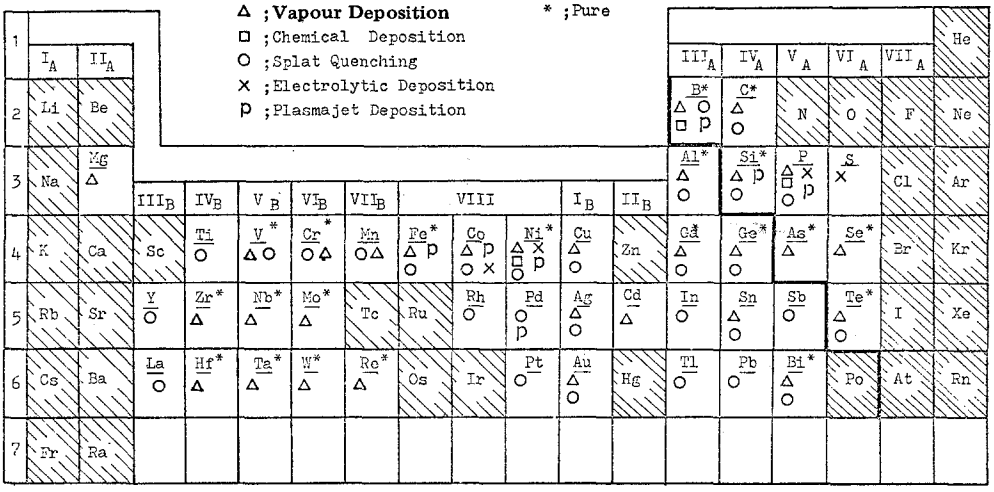

Figure 1 The Periodic Table representation of amorphous elements.

TABLE II Amorphous phases of some materials

System	Composition range x (at. %)	Method	Reference
$Au_{100-x}Si_x$	18.6–30	SQ	[16, 30, 31]
$Au_{75}Pb_{25}$	–	SQ	[32]
$Au_{100-x}Sn_x$	29–31	SQ	[33]
$Au_{73}Ge_{27}$	–	SQ	[34]
$Au_xGe_ySi_z$	x = 74–79 y = 12.4–13.6 z = 8.4–9.4	SQ	[35]
$Ag_{100-x}Si_x$	17–30	SQ	[32]
Ag_xCu_y	x = 35–65 y = 35–50	EV	[36, 37]
$Ag_{100-x}Mn_x$	4–13	EV	[38]
$Al_{82.7}Cu_{17.3}$	–	SQ	[39]
$Al_{100-x}Ge_x$	30–80	EV	[40]
Ge, Te, B	Pure	EV, SQ	[41–43]
As, Bi, C, Ga, Se, Sb, Si	Pure	EV	[15, 42]
Fe, Al, Cr, Pd	Pure	EV	[44–46]
Ni	Pure	EV, SQ	[47, 48]
W, Mo, Ta, Nb, V	Pure	EV	[49–51]
Hf, Zr, Re	Pure	EV	[49]
$Cd_{25}Ge_{25}As_{50}$	–	EV	[52]
$Co_{100-x}Au_x$	25–65	EV	[53]
$Co_{100-x}P_x$	18–25	ED	[54, 55]
$Co_{73}P_{16}B_{12}$	–	P	[25]
$Cu_{100-x}Ti_x$	30–35	SQ	[56]
Cu_xZr_y	x = 60, 57 y = 40, 43	SQ	[57]
Cu–Bi	?	EV	?
$Fe_{84}C_{16}$	–	SQ	[58]
$Fe_xP_yC_z$	x = 75–81 y = 10–16 z = 5–9	SQ, P	[59, 60, 25]
$Fe_{80}P_{13}B_7$	–	P	[25]
$Fe_{76}B_{13}C_7$	–	P	[25]
$Fe_{40}Ni_{40}P_{14}B_6$	–	SQ	[61]
$(Fe_{100-x}Mn_x)_{75}P_{15}C_{10}$	0–10	SQ	[62]
$Fe_{75}P_{16}Si_6Al_3$	–	SQ	[63]
$Fe_{75}P_{15}C_3Al_4$	–	SQ	[61]
$Fe_{77}P_{17}C_4Al_4$	–	SQ	[61]
$Fe_{74}P_{16}C_5Al_3Si_2$	–	SQ	[63, 64]
$Fe_{76}P_{16}C_4Al_2Si_2$	–	SQ	[63. 64]
$Fe_{72}P_{16}C_5Si_2Al_5$	–	SQ	[65]
$Fe_{80-x}Cr_xP_{13}C_7$	0–10	SQ	[66]
$Fe_{80-x}Ni_xP_{13}C_7$	0–40	SQ	[66]
$(Fe_{100-x}Ni_x)_{75}P_{15}C_{10}$	0–50	SQ	[67]
$Fe_{38.5}Ni_{38.5}P_{20-x}B_xAl_3$	2–10	SQ	[61]
$(Fe_{50}Ni_{50})_{80-x}P_{14}B_6A_x$ (A = Si or Al)	1–3	SQ	[61]
$(Fe_{100-x}Ni_x)_{77}P_{14}B_6Al_3$	0–10	SQ	[61]
$(Fe_{50}Ni_{50})_{81-x}P_{16}B_xAl_3$	4–7	SQ	[61]
$(Fe_{50}Ni_{50})_{91-x}P_xB_6Al_3$	14–17	SQ	[61]
$Fe_{80-x}P_{16}C_xB_1Al_3$	3–6	SQ	[61]
$Fe_{76.6}P_{14.2}C_{1.2}B_{4.8}Al_{3.2}$	–	SQ	[61]
$Fe_{70-x}Cr_{10}Ni_xP_{13}C_7$	5–20	SQ	[66]
$(Fe_{75}P_{15}C_6Al_4)_{100-x}(Fe_{77}P_{14}B_6Al_3)_x$	0–10	SQ	[61]
$Gd_{100-x}Co_x$	39–96	SQ	[68, 69]
$Gd_{100-x}Fe_x$	15–94	SQ, EV	[68, 70]

TABLE II continued

TABLE II Amorphous phases of some materials – *continued*

System	Composition range x (at.%)	Method	Reference
$Ge_{100-x}Bi_x$	0–25	EV	[71]
$La_{100-x}Au_x$	0–40	SQ	[72]
La–Cu	?	SQ	[72]
La–Ni	?	SQ	[72]
$Mg_{65}Cu_{35}$	–	EV	[37]
$Mg_{60}Sb_{40}$	–	EV	[73]
Mg–Bi	?	EV	[74]
$Mn_{100-x}Si_x$	23–28	SQ	[75]
$Mn_{75}P_{15}C_{10}$	–	SQ	[62, 76]
$Nb_{100-x}Ni_x$	33–78	SQ	[77]
$Nb_{48}Ni_{39}Al_{13}$	–	SQ	[77]
$Ni_{100-x}P_x$	8.6–26.2	CD, ED, EV	[9–11]
$Ni_{100-x}Ta_x$	35–45	SQ	[77]
$Ni_{80}S_{20}$	–	ED	[9, 10]
Ni–B	?	CD	[10, 11]
$Ni_{75}P_{15}B_{10}$	–	P	[25]
$(Ni_{41}Pd_{41}B_{18})_{100-x}Cr_x$	0–4	SQ	[78]
$Ni_{90-x}P_xB_7Al_3$	16–18	SQ	[63]
$Ni_{49}Fe_{29}P_{14}B_6Al_2$	–	SQ	[64]
$Ni_{72}P_{14}B_6Si_3Al_5$	–	SQ	[65]
$Pb_{75}Au_{25}$	–	SQ	[32]
$Pb_{52}Sb_{48}$	–	SQ	[79]
$Pd_{100-x}Ge_x$	18–20	SQ	[80]
$Pd_{100-x}Si_x$	15–23	P, SQ	[81, 3, 25]
$Pd_{80-x}Cr_xSi_{20}$	0–10	SQ	[82]
$Pd_{80-x}Mn_xSi_{20}$	0–10	SQ	[82]
$Pd_{80-x}Fe_xSi_{20}$	0–10	SQ	[83, 84]
$(Pd_{82}Si_{18})_{100-x}Fe_x$	10–90	SQ	[85]
$(Pd_{100-x}Fe_x)_{83.5}Si_{16.5}$	1–12	SQ	[86]
$Pd_{78}Si_{20}Fe_xCr_{2-x}$	0–2	SQ	[87]
$Pd_{80-x}Co_xSi_{20}$	0–10	P, SQ	[83, 84]
$(Pd_{100-x}Co_x)_{83.5}Si_{16.5}$	0–18	SQ	[86]
$Pd_{80-x}Ni_xSi_{20}$	0–10	SQ	[83]
$(Pd_{100-x}Ni_x)_{83.5}Si_{16.5}$	0–60	SQ	[86]
$Pd_xCu_ySi_z$	x = 65–80 y = 3–19 z = 16–20.5	SQ	[88]
$(Pd_{82.4}Si_{17.6})_{100-x}Cu_x$	0–14	SQ	[89]
$(Pd_{100-x}Cu_x)_{83.5}Si_{16.5}$	0–26	SQ	[89]
$Pd_xAg_ySi_z$	x = 75–79 y = 4–8 z = 16–20	SQ	[88]
$(Pd_{100-x}Ag)_{83.5}Si_{16.5}$	0–18	SQ	[86]
$Pd_xAu_ySi_z$	x = 68–81 y = 4–12 z = 15–20	SQ	[88]
$(Pd_{100-x}Au_x)_{83.5}Si_{16.5}$	0–20 80–100	SQ	[86]
$(Pd_{100-x}Rh_x)_{83.5}Si_{16.5}$	0–6	SQ	[86]
$Pd_{84}Ge_xSi_y$	x = 2–7 y = 10–14 x = 77–79	SQ	[88]
$Pd_xAu_yAg_zSi_{16.5}$	y = 2–15 z = 3–4	SQ	[88]
$(Pd_{70}Mn_{30})_{100-x}P_x$	17–26	SQ	[90]
$Pd_{80-x}Fe_xP_{20}$	10–48	SQ	[7]
$(Pd_{100-x}Co_x)_{80}P_{20}$	15–60 x = 0–82	SQ	[90]

TABLE II continued

TABLE II Amorphous phases of some materials – *continued*

System	Composition range x (at.%)	Method	Reference
$Pd_xNi_yP_z$	y = 8–73 z = 10–23	SQ	[7, 103, 104]
$(Pd_{60-x}Pt_xNi_{40})_{75}P_{25}$	0–60	SQ	[91]
$Pt_{100-x}Ge_x$	17–30	SQ	[92]
$Pt_{100-x}Sb_x$	33–37	SQ	[92]
$Pt_{100-x}Si_x$	23, 25, 68	SQ	[92]
$(Pt_{100-x}Ni_x)_{80}P_{20}$	10–80	SQ	[86]
$(Pt_{100-x}Ni_x)_{75}P_{25}$	20–70	SQ	[93]
$(Pt_{70}Ni_{30-x}Cr_x)_{75}P_{25}$	1.5–6	SQ	[94]
$(Pt_{70}Ni_{30-x}V_x)_{75}P_{75}$	0–3	SQ	[95]
$Rh_{78}Si_{22}$	–	SQ	[92]
Rh–Ge	?	SQ	[92]
$Sn_{90}Cu_{10}$	–	SQ, EV	[13, 14]
$Te_{100-x}Ga_x$	10–30	SQ	[96–98]
$Te_{100-x}Ge_x$	10–25	SQ	[96–98]
$Te_{100-x}In_x$	10–30	SQ	[96–98]
$Te_{70}Cu_{25}Au_5$	–	SQ	[84]
$Tl_{100-x}Te_x$	15–60	EV, SQ	[99, 100]
$Tl_{100-x}Au_x$	25–60	SQ	[101]
$Zr_{72}Co_{28}$	–	SQ	[56]
$Zr_{100-x}Ni_x$	20–40	SQ	[56]
$Zr_{100-x}Cu_x$	40–75	SQ	[56]
$Zr_{100-x}Pd_x$	20–35	SQ	[56]
Y–Fe	?	SQ	[102]

Notes: EV = vapour deposition, ED = electrolyte deposition, CD = chemical deposition (electroless), P = plasma-jet deposition, SQ = splat quenching

numbers are selected and listed in chronological order for each alloy. These results, however, are presented in the Periodic Table (Fig. 1) including the method of production. An asterisk denotes an amorphous material obtained even with the pure elements. Metalloids and semi-metal elements have a great tendency to produce amorphous phases; generally, the elements which form amorphous alloys are noble and some transition metals (those with nearly occupied d bands) as host, while the metalloid and more electropositive elements form as the solute. The composition range of this group of alloys falls in the vicinity of 20 at.% metalloid. It is also noticeable that even alloys mixed with only noble or transition metals can form amorphous phases in the systems Sn–Cu [13, 14], Cu–Ag [36, 37], Au–Co [53], etc., which have deep eutectic compositions in the phase diagrams. Such a tendency to form an amorphous material will be discussed in the later section.

4. Properties of amorphous alloys

It is well known that a homogeneous solid solution alloy can be achieved by rapid quenching from the liquid state and, moreover, that the solubility of a solid solution may be extended by using this method (Falkenhagen and Hofmann [15]). Most of the solid solutions produced by this method satisfy the Hume–Rothery rule [19]. However, metastable crystalline phases and amorphous (non-crystalline) phases can also be obtained by quenching from the liquid state [16, 106].

Amorphous phases in alloys can be characterized by their X-ray diffraction intensity curve which has a broad main peak, sharper and stronger than that of a liquid. In addition there are usually three or four very weak subpeaks [2–7]. It is particularly interesting that the second subpeak in the X-ray intensity curves for some amorphous alloys

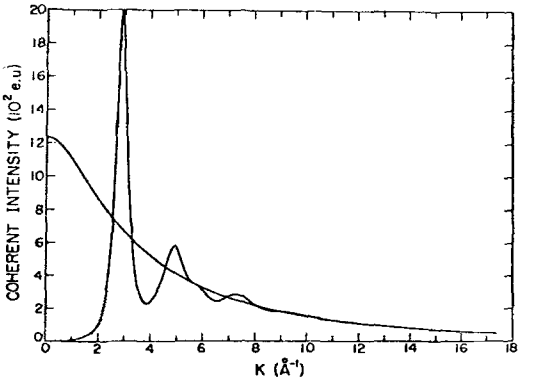

Figure 2 X-ray diffraction pattern of an $(Ni_{50}Pd_{50})_{85}P_{15}$ amorphous alloy [108].

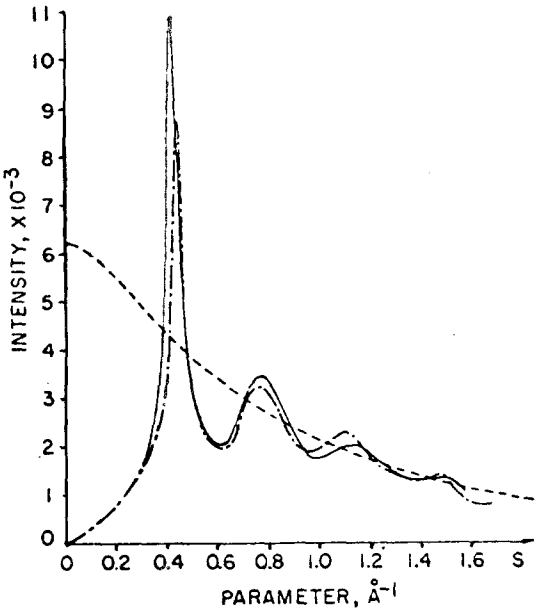

Figure 3 Coherent intensity curves of an amorphous $Au_{70}Si_{30}$ alloy (solid line) and liquid gold (dashed line) [107].

(excluding Au–Si [107], Ni–Pt–P [5] and certain Ni–Pd–P systems [108]) have shoulder peaks in the second subpeaks, i.e. overlapping strong and weak peaks, which do not appear in liquid metal intensity curves. This is illustrated in Figs. 2 and 3. Accordingly, the diffraction pattern in TEM for amorphous alloys shows a rather intense diffuse halo associated with a few weak, almost invisible rings. Fig. 4 shows a typical bright-field transmission electron micrograph of a $Ni_{55}Pd_{35}P_{10}$ amorphous alloy and the diffraction pattern corresponding to it. The narrow, dark section in the bright-field micrograph shows a crack in the thin film. As indicated in Fig. 4, the bright-field image does not have contrast normally found in crystalline materials (such as bend contours). However, the dark-field images in many cases show tiny bright spots corresponding to strong coherent scattering regions (see the amorphous region in Fig. 5b). Using high resolution electron micrographs, both dark-field and interference pictures of the amorphous Ge films revealed that the size of these bright specks may indicate microcrystals with a diameter of about 14 Å [109]. The calculation of the radial distribution function has also predicted that regions of S.R.O. over about 15 Å may exist in metal glasses [2–7]. Subsequently, these investigations indicated that the investigations indicated that the perfect amorphous state, whose atomic arrangement is completely random with no short range order, does not exist in metal glasses. Therefore, to distinguish between an amorphous phase and microcrystalline phase, we define the amorphous state as that where short range order exists over a region of less than about 15 ± 1 Å. Fig. 5 shows two kinds of microcrystal morphologies which were found in some $Ni_{55}Pd_{35}P_{10}$ samples, which failed to form an amorphous phase. Fig. 5a indicates the bright-field and Fig. 5b the dark-field image. The former shows about 50% of the partially crystallized amorphous phase and the latter only a few per cent. In both cases the metastable crystalline phase is embedded in the amorphous phase. The transmission electron micrographs of the 50% partially crystallized sample (a) shows a large dendritic crystalline growth. The partially crystallized sample (b) shows a spherulite growth similar to some polymers [110].

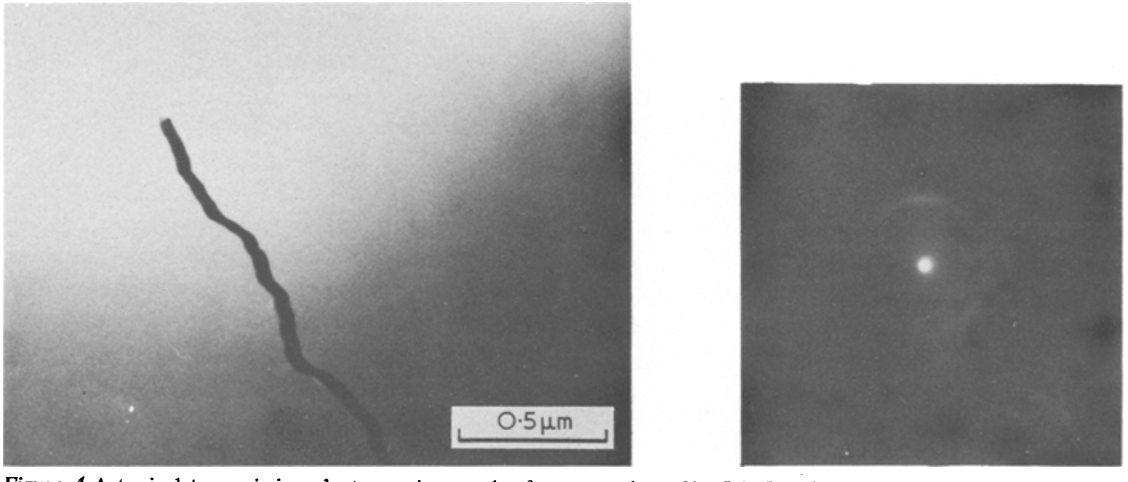

Figure 4 A typical transmission electron micrograph of an amorphous $Ni_{55}Pd_{35}P_{10}$ alloy (bright-field) and the corresponding diffraction pattern.

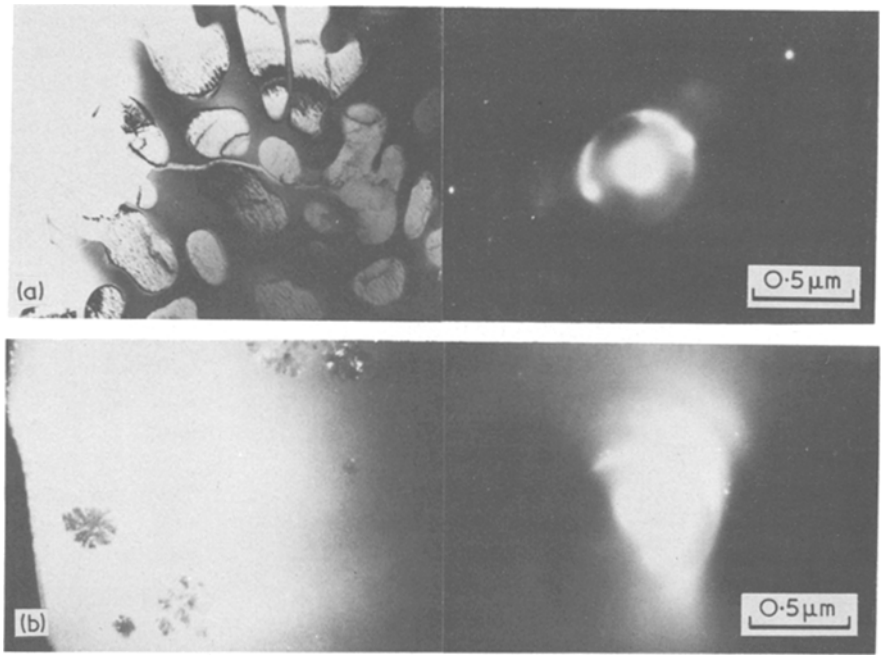

Figure 5 Transmission electron micrographs of partially crystallized $Ni_{55}Pd_{35}P_{10}$ alloy: (a) about 50% partial crystallization (bright-field) and (b) a few % partial crystallization (dark-field).

The random atomic arrangement of amorphous alloys has also been supported by the fact that the spontaneous Hall coefficient of amorphous alloy is almost independent of temperature [111] and also by the fact that the Mössbauer spectrum can be explained by a disordered alloy model in which the interatomic distance has a spread in values [112].

The transition from liquid to glass has been defined by the marked change of the viscosity, specific heat and thermal expansion within a narrow temperature interval around a glass transition temperature. In addition, this solidification from a liquid to a glass is charactertized in a continuous sense, e.g. as the temperature decreases across the glass temperature (T_g), the viscosity increases rapidly but continuously, while at the same time the specific volume and the configurational entropy decrease continuously. This is remarkably different from the crystalline state where the viscosity, specific volume and the entropy change discontinuously. The temperature dependence of fluidity, ϕ ($\phi = 1/\eta$), where η is the coefficient of viscosity, is shown in Fig. 6. The reduced temperature τ is expressed as:

$$\tau = kT/h_v \qquad (1)$$

where k is the Boltzmann constant and h_v is the heat of vaporization. The fluidity of a simple Van

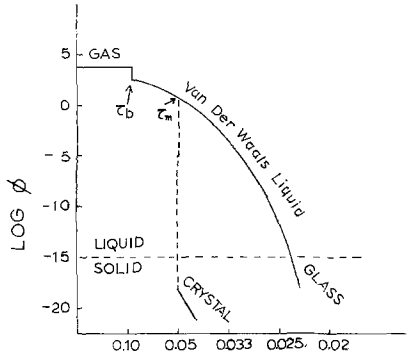

Figure 6 Relation between fluidity and reduced temperature for a simple glass forming liquid. The dashed line is a crystalline liquid [113].

Der Waals liquid decreases rapidly near T_g and results in the freezing of the liquid into an amorphous state. These transitions are schematically illustrated in Figs. 7 and 8 which show the temperature dependence of specific volume and entropy respectively. These indicate that the magnitude of these properties always remain larger in the amorphous than in the crystalline state. The liquid region between T_m and T_g in both figures is referred to as a supercooled liquid. In the actual case of an amorphous alloy, the density change of the amorphous phase to the crystalline state is less than 1 to 2% [89, 115]. This indicates that amorphous alloys have dense atomic packing close to

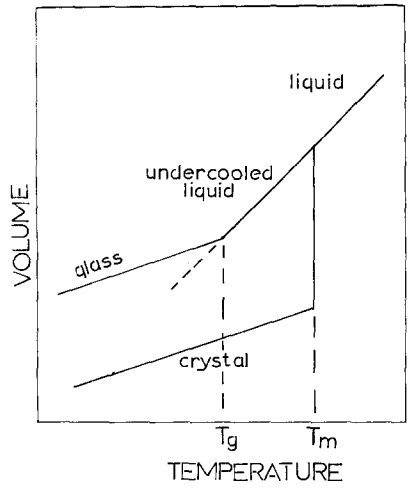

Figure 7 Schematic illustration of the relation between specific volume and temperature for an ideal glass forming system. [3].

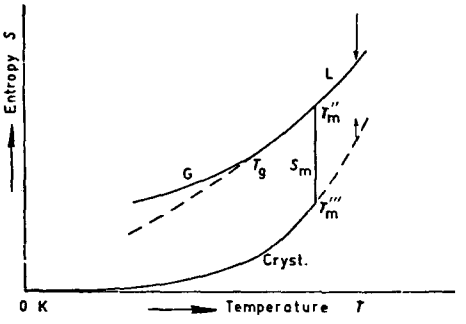

Figure 8 Schematic representation of the entropy versus temperature curve for a glass forming system [114].

that of the crystalline state. In Fig. 8 it is interesting to ask whether amorphous solids obey Nernst's third law, i.e. entropy becomes zero at 0 K. From the point of view of the above argument the liquid–glass transition could be classified as a second-order phase transition (in the sense of Ehrenfest) which is defined as a discontinuity in the second order derivative of the free energy. For example, a discontinuity of the heat capacity. Gibbs and Dimarzio [116] pointed out that the configurational entropy will vanish in a hypothetical glass at the thermodynamic second-order transition temperature T_2. T_2 would be obtained on an infinite time scale which, therefore, results in a lower limit to the glass temperature T_g, obtained experimentally over a finite time. Accordingly, below T_2 the system will remain in one of its configurations referred to the ground state. Since the difference between the vibrational entropy of the glass and crystal is very small, the difference between the total entropy of the glass and crystal at $T = 0$ K, e.g. a zero point entropy ΔS_0, may be equal, with a good approximation, to the configurational entropy of the liquid which was frozen in at T_g:

$$\Delta S_0 = S_{\text{conf.}}(T_g).$$

Therefore, it has a finite entropy value at $T = 0$ K [117]. In an actual case, however, T_2 is close to T_g, so that we might define the configurational entropy as nearly zero at T_g [118]. Theoretically, this glass temperature T_g is attributed to either (a) the temperature below which the relaxation time is too long for the equilibrium state to be reached in a finite time [117], or (b) the temperature at which the probability of finding the critical local concentration of free volume required for a viscous flow will vanish [113]. As stated above, this transition is characterized by no structural change but a small volume change. Thermodynamically, T_g is considered as the temperature at which the meaningless negative entropy terminates when the temperature decreases from the liquid state to the solid state. This was first pointed out by Kauzmann [119]. This entropy may be referred to as the structural configurational entropy, resulting in a major role for the excess heat capacity ΔC_p ($\Delta C_p = C_p^l - C_p^m$, where C_p^l and C_p^m are designated as the heat capacities of the liquid and the mixing equilibrium solid respectively) [30]. Experimentally, however, T_g is determined either as the temperature where the viscosity reaches a certain value, i.e. 10^{13} P in most cases [120, 121] or as temperature at the point of inflection in C_p–T curves. The specific heat, C_p, of a $Au_{76.89}Ge_{13.66}Si_{9.45}$ amorphous alloy is plotted versus temperature in Fig. 9, where l, g and m denote the liquid, glass and solid mixture respectively [35]. The solid lines indicate experimental results. C_p^g is slightly larger than C_p^m below T_g, rises steeply near T_g (= 297 K) over a narrow range, ~5 K, as the temperature is increased and then coinciding with the curve extrapolated from the stable and supercooled liquid. The decrease of C_p^l with increasing temperature results in an increasing configurational entropy [122]. Since the entropy of melting, ΔS_f, of the equilibrium mixture can be described as:

$$\Delta S_f(T) = \Delta S_f(T_f) + \int_{T_f}^{T} \frac{C_p}{T}\,dT \qquad (2)$$

where f denotes fusion and $\Delta C_p = C_p(l) - C_p(S)$, ΔS_f becomes zero and then negative if the increase in C_p continues with decreasing temperature, as

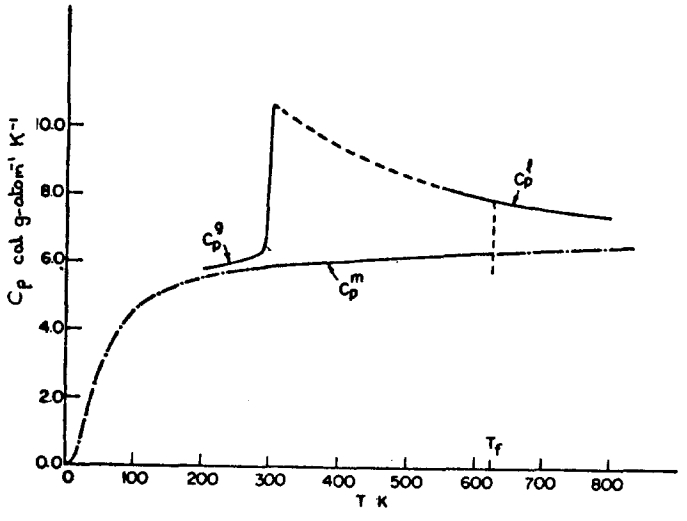

Figure 9 Temperature dependence of the specific heat, C_p, for $Au_{76.79}Si_{9.45}Ge_{13.66}$ amorphous alloys, 1, g and m denote the liquid, glass and solid mixture respectively: T_f(= 625 K), is the melting point of the mixture [35].

shown in Fig. 9. The melting entropy at $T = 290$ K for this amorphous alloy was calculated to be $\Delta S_f(290\,\text{K}) = 1.47 \pm 0.16$ cal g-atom^{-1} K^{-1}, which is 36% of $\Delta S_f(T_f = 625\,\text{K}) = (4.07$ cal g-atom^{-1} K^{-1}) and only 7.3% larger than that of the ideal mixing entropy (1.36 cal g-atom^{-1} K^{-1} for this composition). Consequently, the entropy of amorphous alloys below T_g consists mostly of the entropy of mixing and thermal entropy leaving only a small contribution from the non-compositional configurational parts. It is worthwhile remarking that the C_p^g curve is reversible below the temperature at which spontaneously crystallization occurs [35].

5. Formation and stability criterion

Cohen and Turnbull [123] first pointed out that the amorphous structure is thermodynamically metastable. Later, Weaire *et al.* [124] have demonstrated that the glass is metastable, since it is stable with respect to infinitesimal distortions, but has higher energy than that of the crystal (this resulted from the calculation based on the assumption of a pair potential and on the use of both the Finney's D.R.P. [125] and Cargill's [4] experimental radial distribution function). The formation and stability of amorphous alloys have been studied for almost two decades. These have been discussed with the concepts of the alloying effect (including impurity), size effect, configurational entropy, ΔS, and mixing enthalpy, ΔH, (quasi-chemical approach), and chemical bonding [17]. Thus I would like, in turn, to review and discuss these problems in this section.

5.1. Alloying effect

It is well known that a fast cooling rate is a sufficient condition for by-passing crystallization during solidification and producing an amorphous state [19, 126]. This has been further demonstrated by Uhlmann [127] and Davies *et al.* [128] in their studies of kinetics of formation of glassy metals, and more recently in terms of solidification and crystal growth rate [129]. The phases present after quenching in terms of either the cooling rate, R [130], or the supercooled temperature, ΔT_s, are shown in Fig. 10 for the Au–Ge system, where ΔT_s is measured from the equilibrium liquidus temperature. Fig. 11 shows the equilibrium phase diagram of the Au–Ge alloy system [131]. From Figs. 10 and 11, it is seen that near the deep eutectic composition, metal glasses may be easily obtained with a relatively low cooling rate or ΔT_s.

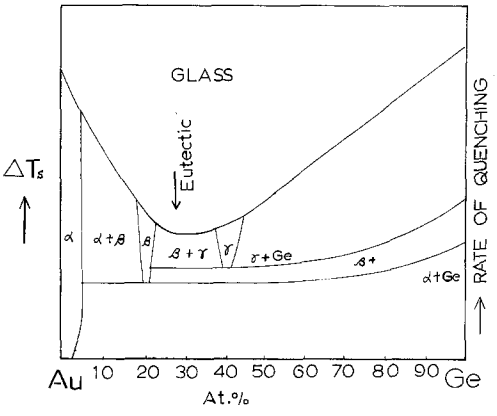

Figure 10 Dependence of quenched in phases on the super cooling temperature or the cooling rate for Au–Ge system [130].

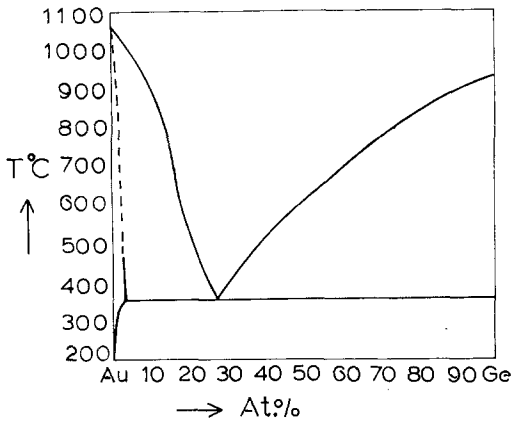

Figure 11 Equilibrium phase diagram in the Au–Ge system [131].

Furthermore, a large cooling rate or super quenching is required to produce a pure element in the amorphous state. In Fig. 10 it is also indicated that glass formation is favoured at the composition where stable or metastable phases do not exist. However, natural oxide glasses, chalcogenide glasses and amorphous polymers can be obtained even at low cooling rates or ΔT_s, while it is also reported in some alloy systems we can easily achieve on amorphous state only with quenching in water ($\sim 10^{2\circ}$ C sec^{-1} cooling rate) [86, 88]. Thus from these facts, it is plausibly concluded that the rapid cooling rate is not a necessary condition in obtaining amorphous states.

To help our further discussion, Table II is rewritten in terms of the Goldschmidt atomic radii, the electronegativity and the group of the table for each element. These are shown in Table III. Before Duwez and his colleagues developed the new splat quenching technique [16], evaporation methods were used extensively for the preparation of amorphous materials. These evaporation techniques, actually, have the following advantages: good thermal conductivity to absorb the heat of condensation can be, on the one hand, achieved easily by cooling the substrate with liquid nitrogen, which also reduces thermal diffusion, and on the other hand, a random and homogeneous solid solution can easily be obtained for systems which have essentially no solubility in the solid or liquid state since the vapour phase has no miscibility restriction. It is interesting to note that a crystalline substrate enhances the possibility of obtaining a crystalline film and an amorphous substrate on amorphous film [132]. This evidence was described by using D.R.P. [133, 134] and suggests that a periodic potential in the crystalline substrate causes a great restriction on the site selection of the incoming atoms.

Looking at the group column of Table III we see that generally noble and some transition metals are host elements, while metalloid and more electropositive elements are solutes. Yet as stated in Section 3, alloys consisting of noble, transition, or no transition metal only can be obtained in amorphous states, as presented in Table II. In most cases these alloys have deep eutectic compositions. In contrast to this evidence, some amorphous alloys present after quenching exist far from the eutectic composition: for example, Co–Au, Zr–Co, Tl–Te and Au–Pb. Moreover, one can obtain the amorphous state even in the intermetallic compound, which may have large negative mixing enthaply, ΔH_m, i.e. Cu_3Zr_2, Mg_3Sb_2, etc. and in the alloy systems with negligible eutectic compositions, i.e. Ge–Bi and Cu–Bi (see Table III). It is obvious from the foregoing that one has to consider other factors in predicting the occurrence of the amorphous state.

A number of pure metalloid and metal elements have been obtained in amorphous states by vapour deposition or splat quenching. Particularly the amorphous state of pure metalloid elements is favoured over that of pure metallic cases. This has been explained by the diffusion distance of crystallization due to the bonding structures and the atomic mobility in condensation [135]. It is also reported that gaseous impurities, for example, O_2 and N_2, increase the tendency of forming an amorphous material and also help stabilize the structure [44, 135, 136], although on splat-quenching, some care must be taken to minimize oxidation to achieve a high cooling rate [39(b)].

The glass forming tendency and the stability are generally described by means of the following parameters:

$$\Delta T_g = T_m - T_g \quad \text{and} \quad \Delta T_c = T_c - T_g$$

where T_m, T_g and T_c denote the melting, glass and crystallization temperature respectively. For known amorphous alloys, T_m is always greater than T_g, while T_c is near T_g (in most cases, within 50° C greater than T_g) [86, 88, 89]. As the temperature decreases from T_m, the rate of the crystallization will increase rapidly. However, in most amorphous alloys appreciable crystallization does not occur on isochronal annealing below T_g. Thus, the maximum crystallization rate should exist between T_g and T_m. A schematic illustration is shown in Fig.

TABLE III Comparison of atomic radii and electro-negativity in some amorphous alloy systems

System	Groups	Goldschmidt radii (12-fold) (Å)	$\frac{R_1-R_2}{R_1}$ (%)	Degree of electro-negativity	Method
Au–Si	I_B–IV_A	1.44–1.32	8.3	2.4–1.8	SQ
Au–Ge	I_B–IV_A	1.44–1.37	4.9	2.4–1.8	SQ
Au–Sn	I_B–IV_A	1.44–1.62	−12.5	2.4–1.8	SQ
Au–Pb	I_B–IV_A	1.44–1.75	−21.5	2.4–1.8	SQ
Au–Ge–Si	I_B–IV_A–IV_A	1.44–1.37–1.32	8.3	2.4–1.8–1.8	SQ
Ag–Mn	I_B–VII_B	1.44–1.30	9.7	1.9–1.5	EV
Ag–Si	I_B–IV_A	1.44–1.32	8.3	1.9–1.8	SQ
Ag–Cu	I_B–I_B	1.44–1.28	11.1	1.9–1.9	EV
Al–Cu	III_A–I_B	1.43–1.28	10.5	1.5–1.9	SQ
Al–Ge	III_A–IV_A	1.43–1.37	4.2	1.5–1.8	EV
Cd–Ge–As	II_B–IV_A–V_A	1.52–1.37–1.39	8.6	1.7–1.8–2.0	EV
Co–Au	VIII–I_B	1.25–1.44	−15.2	1.8–2.4	EV
Co–P	VIII–V_A	1.25–1.28	−2.4	1.8–2.1	ED
Co–P–B	VIII–V_A–III_A	1.25–1.28–0.97	22.4	1.8–2.1–2.0	P
Cu–Ti	I_B–IV_B	1.28–1.47	−14.8	1.9–1.5	SQ
Cu–Zr	I_B–IV_B	1.28–1.60	−25.0	1.9–1.4	SQ
Cu–Bi	I_B–V_A	1.28–1.70	−32.8	1.9–1.9	EV
Fe–C	VIII–IV_A	1.27–1.42	−11.8	1.8–2.5	SQ
Fe–P–B	VIII–V_A–III_A	1.27–1.28–0.97	23.6	1.8–2.1–2.0	P
Fe–B–C	VIII–III_A–IV_A	1.27–0.97–1.42	−11.8	1.8–2.0–2.5	P
Fe–P–C	VIII–V_A–IV_A	1.27–1.28–1.42	−11.8	1.8–2.1–2.5	SQ, P
Fe–P–C–Cr	VIII–V_A–IV_A–VI_B	1.27–1.28–1.42–1.27	0	1.8–2.1–2.5–1.6	SQ
Fe–P–C–Mn	VIII–V_A–IV_A–VII_B	1.27–1.28–1.42–1.30	−2.4	1.8–2.1–2.5–1.5	SQ
Fe–P–C–Ni	VIII–V_A–IV_A–VIII	1.27–1.28–1.42–1.24	2.4	1.8–2.1–2.5–1.8	SQ
Fe–P–C–Al	VIII–V_A–IV_A–III_A	1.27–1.28–1.42–1.43	12.6	1.8–2.1–2.5–1.5	SQ
Gd–Co	VIII–VIII	1.80–1.25	30.6	−1.8	SQ
Gd–Fe	VIII–VIII	1.80–1.27	29.4	−1.8	SQ
Ge–Bi	IV_A–V_A	1.37–1.70	−24.1	1.8–1.9	EV
La–Au	III_B–I_B	1.88–1.44	33.5	1.1–2.4	SQ
La–Cu	III_B–I_B	1.88–1.28	31.9	1.1–1.9	SQ
La–Ni	III_B–VIII	1.88–1.25	33.5	1.1–1.8	SQ
Mg–Cu	II_A–I_B	1.60–1.28	20.0	1.2–1.9	EV
Mg–Sb	II_A–V_A	1.60–1.59	0.6	1.2–1.9	EV
Mg–Bi	II_A–V_A	1.60–1.70	−6.3	1.2–1.9	EV
Mn–Si	VII_B–IV_A	1.30–1.32	−1.5	1.5–1.8	SQ
Mn–P–C	VII_B–V_A–IV_A	1.30–1.28–1.42	−9.3	1.5–2.1–2.5	SQ
Nb–Ni	V_B–VIII	1.47–1.25	15.0	1.6–1.8	SQ
Nb–Ni–Al	V_B–VIII–III_A	1.47–1.25–1.43	2.7	1.6–1.8–1.5	SQ
Ni–B	VIII–III_A	1.25–0.97	22.4	1.8–2.0	CD
Ni–P	VIII–V_A	1.25–1.28	−2.4	1.8–2.1	CD, ED, EV
Ni–S	VIII–VI_A	1.25–1.04	16.8	1.8–2.5	ED
Ni–Ta	VIII–V_B	1.25–1.46	−16.8	1.8–1.5	SQ
Ni–P–B	VIII–V_A–III_A	1.25–1.28–0.97	22.4	1.8–2.1–2.0	P
Ni–Pd–B–Cr	VIII–VIII–III_A–VI_B	1.25–1.37–0.97–1.27	−1.6	1.8–2.2–2.0–1.6	SQ
Ni–Pd–B–Al	VIII–V_A–III_A–III_A	1.25–1.28–0.97–1.43	−14.4	1.8–2.1–2.0–1.5	SQ
Pb–Sb	IV_A–V_A	1.75–1.59	9.1	1.8–1.9	SQ
Pb–Au	IV_A–I_B	1.75–1.44	17.7	1.8–2.4	SQ

TABLE III continued

TABLE III Comparison of atomic radii and electro-negativity in some amorphous alloy systems – *continued*

System	Groups	Goldschmidt radii (12-fold) (Å)	$\frac{R_1 - R_2}{R_1}$ (%)	Degree of electro-negativity	Method
Pd–Ge	VIII–IV_A	1.37–1.37	0	2.2–1.8	SQ
Pd–Si	VIII–IV_A	1.37–1.32	3.6	2.2–1.8	SQ, P
Pd–Si–Cr	VIII–IV_A–VI_B	1.37–1.32–1.27	7.3	2.2–1.8–1.6	SQ
Pd–Si–Mn	VIII–IV_A–VII_B	1.37–1.32–1.30	5.1	2.2–1.8–1.5	SQ
Pd–Si–Fe	VIII–IV_A–VIII	1.37–1.32–1.27	7.3	2.2–1.8–1.8	SQ
Pd–Si–Co	VIII–IV_A–VIII	1.37–1.32–1.25	8.8	2.2–1.8–1.8	SQ
Pd–Si–Ni	VIII–IV_A–VIII	1.37–1.32–1.24	9.5	2.2–1.8–1.8	SQ
Pd–Si–Rh	VIII–IV_A–VIII	1.37–1.32–1.34	2.2	2.2–1.8–2.2	SQ
Pd–Si–Cu	VIII–IV_A–I_B	1.37–1.32–1.28	6.6	2.2–1.8–1.9	SQ
Pd–Si–Ag	VIII–IV_A–I_B	1.37–1.32–1.44	– 5.1	2.2–1.8–1.9	SQ
Pd–Si–Au	VIII–IV_A–I_B	1.37–1.32–1.44	– 5.1	2.2–1.8–2.4	SQ
Pd–Si–Ge	VIII–IV_A–IV_A	1.37–1.32–1.37	0	2.2–1.8–1.8	SQ
Pd–Si–Au–Ag	VIII–IV_A–I_B–I_B	1.37–1.32–1.44–1.44	– 5.1	2.2–1.8–2.4–1.9	SQ
Pd–Si–Fe–Cr	VIII–IV_A–VIII–VI_B	1.37–1.32–1.27–1.24	9.5	2.2–1.8–1.8–1.6	SQ
Pd–P–Mn	VIII–V_A–VII_B	1.37–1.28–1.30	5.1	2.2–2.1–1.5	SQ
Pd–P–Fe	VIII–V_A–VIII	1.37–1.28–1.27	7.3	2.2–2.1–1.8	SQ
Pd–P–CO	VIII–V_A–VIII	1.37–1.28–1.25	8.8	2.2–2.1–1.8	SQ
Pd–P–Ni	VIII–V_A–VIII	1.37–1.28–1.24	9.5	2.2–2.1–1.8	SQ
Pd–Pt–Ni–P	VIII–VIII–VIII–V_A	1.37–1.38–1.24–1.28	6.6	2.2–2.2–1.8–2.1	SQ
Pt–Si	VIII–IV_A	1.38–1.32	4.3	2.2–1.8	SQ
Pt–Ge	VIII–IV_A	1.38–1.37	0.7	2.2–1.8	SQ
Pt–Sb	VIII–V_A	1.38–1.59	– 15.2	2.2–1.9	SQ
Pt–Ni–P	VIII–VIII–V_A	1.38–1.24–1.28	7.2	2.2–1.8–2.1	SQ
Pt–Ni–Cr–P	VIII–VIII–VI_B–V_A	1.38–1.24–1.24–1.28	7.2	2.2–1.8–1.6–2.1	SQ
Pt–Ni–V–P	VIII–VIII–V_B–V_A	1.38–1.24–1.34–1.28	7.2	2.2–1.8–1.6–2.1	SQ
Rh–Si	VIII–IV_A	1.34–1.32	1.5	2.2–1.8	SQ
Rh–Ge	VIII–IV_A	1.34–1.37	– 2.2	2.2–1.8	SQ
Sn–Cu	IV_A–I_B	1.62–1.28	21.0	1.8–1.9	SQ, EV
Te–Ga	VI_A–III_A	1.60–1.41	11.9	2.1–1.6	SQ
Te–In	VI_A–III_A	1.60–1.68	– 5.0	2.1–1.7	SQ
Te–Ge	VI_A–IV_A	1.60–1.37	14.4	2.1–1.8	SQ
Te–Cu–Au	VI_A–I_B–I_B	1.60–1.28–1.44	20.0	2.1–1.9–2.4	SQ
Tl–Au	III_A–I_B	1.71–1.44	15.8	1.8–2.4	SQ
Tl–Te	III_A–VI_A	1.71–1.60	6.4	1.8–2.1	EV, SQ
Y–Fe	III_B–VIII	1.80–1.27	29.4	1.2–1.8	SQ
Zr–Co	IV_B–VIII	1.60–1.25	21.9	1.4–1.8	SQ
Zr–Ni	IV_B–VIII	1.60–1.24	22.5	1.4–1.8	SQ
Zr–Pd	IV_B–VIII	1.60–1.37	14.4	1.4–2.2	SQ
Zr–Cu	IV_B–I_B	1.60–1.28	20.0	1.4–1.9	SQ

Notes: R_1, R_2 = the Goldschmidt atomic radius of the left and right hand elements, respectively, in the system.

12. Accordingly, if one could rapidly quench a molten alloy to a temperature below T_g, a quasi-equilibrium amorphous phase could be obtained. In other words, this indicates that the probability of obtaining an amorphous state is increased as ΔT_g decreases. Thus any factor which causes the rising of the glass temperature and/or the lowering of the melting temperature might affect the formation of the amorphous state. On the other hand, increasing T_c with respect to T_g will result in greater stability for the amorphous state due to an

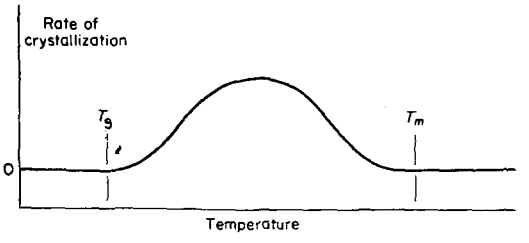

Figure 12 Schematic representation of the relation between the rate of crystallization and the temperature.

increasing ΔT_c. Consequently, the amorphous alloy which has a relatively high T_g and furthermore a large ΔT_c, would be more stable. From the foregoing, the gaseous impurities effect on the formation of amorphous material and its stability could be at least attributed to a decreasing ΔT_g and an increasing T_c. It is interesting to note that the case of obtaining an amorphous material does not always mean that this alloy will be stable [86]. In other words, there is no direct relation between the stable amorphous alloy and those alloys which are easily produced. This suggests that the formation and stability of amorphous alloy may be governed by slightly different mechanisms [86]. Actually, the change of T_c due to alloying with other elements does not follow the change of T_g [86, 88]. The morphology of the crystalline phase which appears during the annealing of an amorphous alloy is often different from that obtained in rapid quenching [104]. These facts also support the above argument.

5.2. Size effect

The fourth column in Table III shows the size difference between constituent atoms in present amorphous alloys. Nowick and Mader predicted that the atomic size difference of constituents was the primary influence in the formation and stability of amorphous alloys [132, 137, 138]. It appeared that an atomic size difference greater than 10% should exist as a requirement for the formation of amorphous phases at 77 K. However, even in systems with atomic size differences less than 10% an amorphous state has been produced: for example, the systems in Pd–Si, Al–Ge, Mg–Bi, etc. Consequently, the possibility of producing amorphous alloys does not depend on the criterion of the atomic size difference in a simple way. Table III also shows, however, that the constituents with about 10 to 20% atomic size difference remarkably extends the composition range in the formation of the amorphous phases. These constituents are not necessarily inter-transition elements but only unlike atoms. These results show that large atomic size differences significantly increase the ease of formation and the stability of amorphous alloys. The atomic size effect has been discussed kinetically [4, 8, 137] and thermodynamically [86, 139, 140]. Computer calculations using hard spheres with different radii indicate negative excess volume and positive entropy with constant pressure, resulting in a lower free energy for the mixture compared with the corresponding case of uniform spheres with a single radius [139, 141]. Furthermore, filling spaces between the random packed hard spheres by atoms with small radii could result in closer packing than that with atoms having uniform hard sphere radii [4, 8]. Hence it appeared that non-uniform atomic sizes kinetically retarded crystal growth and stabilized the amorphous state [137]. Applying a free volume model [113, 142, 143] a fluidity, ϕ, is expressed in the form

$$\phi = A \exp(-k/V_f) \tag{3}$$

where A and K are constants and V_f denotes a free volume. The relation between the fluidity and the self-diffusion coefficient for liquids approximately follows the Stokes–Einstein relation [144, 145];

$$D = (kT/3\pi r_0)\phi \tag{4}$$

where r_0 is a molecular diameter. This relation may also be extended into the glass forming region to a good approximation (empirically up to 10^9 p) [146, 147]. Thus, a more dense random packing with different atomic sizes results in a decreasing free volume, and from Equations 3 and 4, a decreasing fluidity and diffusion coefficient. However, this does not generally hold in actual cases [146, 148–150], i.e. the viscosity of the liquid alloys versus the alloying composition has shown a negative deviation even though the excess molar volume of the alloys may be negative. This has also been demonstrated for the dependence of T_g on admixture of the transition metals, Pd, and Pt with Ni in Pd–Ni–P and Pt–Ni–P amorphous alloys at fixed phosphorous concentration [140]. It revealed a negative deviation of the glass transition temperature with transition metal content. This result predicts that the viscosity of liquid alloys near T_g decreases on the replacement of Pd and Pt with Ni. Hence these results cannot be explained by a simple free volume calculation.

Alder [139] pointed out, however, that in the determination of excess properties, the constituent size differences in ordinary mixtured liquids is of secondary importance to the difference in the attractive potential. In fact, Chen very recently predicted that the excess configurational entropy with random mixing of different atomic sizes, as opposed to the free volume, will lower the viscosity in the liquid alloys, and hence T_g and T_c [86, 140]. In addition, the misfit elastic energy which is always positive, has also been taken into

consideration in reducing the melting temperature T_m [86]. In fact, large size differences in the Au–Ni alloy system seem largely to contribute to the positive mixing enthalpy [151]. On the other hand, using the free volume model [126, 152, 153], the internal free volume is also reflected in the excess configurational entropy.

It is noteworthy that a large atomic size difference in a binary alloy tends to enhance ordering [151]. In contrast, it is suggested that the presence of P which has a smaller radius than the metallic atom increases the local disorder in $(Pd_{50}Ni_{50})_{1-x}P_x$ amorphous alloys [108].

Turnbull [154] calculated the steady frequency of homogeneous nucleation I, and the speed, U, which the crystalliquid advances in the case of super cooled liquids as:

$$I = \frac{K_n}{\eta} \exp\left[-b\alpha^2\beta/T_r(\Delta T_r)^2\right] \quad (5)$$

$$U = \frac{K'}{\eta}\left[1 - \exp\left(-\beta\Delta T_r/T_r\right)\right] \quad (6)$$

with some assumptions, where K_n and K' are kinetic constants, b is a nucleus shape constant, $T_r = T/T_m$, is a reduced temperature, where T_m is the melting temperature, $\Delta T_r = 1 - T_r$, α and β are dimensionless parameters defined as:

$$\alpha = \frac{(N\bar{V}^2)^{1/3}\sigma}{\Delta H_m} \quad (7)$$

$$\beta = \frac{\Delta H_m}{RT_m} = \frac{\Delta S_m}{R} \quad (8)$$

where N is Avogado's number, $\bar{V}$ is the molar volume of the crystal, ΔH_m is the molar heat of fusion, σ is the liquid–crystal interfacial tension, ΔS_m is the molar entropy of fusion and R is the gas constant. Since the rate of crystallization of liquids is specified by I and U, the formation tendency of amorphous states should increase as the fluidity or the kinetic constants K_n, K' (due to the atomic rearrangement) decrease. Also the formation tendency depends strongly on α and β, ΔT_r or the cooling rate. If both I and U, at a given ΔT_r, scale as the fluidity ($\phi = 1/\eta$), the glass forming tendency should also increase as the reduced glass temperature, $T_{r,g}$ ($= T_g/T_m$) increases.

5.3. Configurational entropy

From the above viewpoints, the configurational entropy is presumably more suitable than any other parameter when the formation and stability of amorphous phases are considered. As mentioned above, Adam and Gibbs [117] have developed the statistical-mechanical entropy model in glass-forming liquids. This model derives the following equations, for the average cooperative transition probability $\bar{W}(T)$ per mole,

$$\bar{W}(T) = \bar{A}\exp\left(-\Delta\mu S_c^*/KTS_c\right) \quad (9)$$

where $\bar{A}$ is a frequency factor, approximately independent of temperature, $\Delta\mu$ is essentially the height of the potential energy barrier per monomer for a polymer or atom for an alloy, k is the Boltzmann constant, S_c is the configurational entropy and S_c^* is a critical configurational entropy necessary for the reaction to take place and is related to a critical cooperative region size Z^* by the following equation:

$$Z^* = NS_c^*/S_c \quad (10)$$

where N is the Avogado's number. In fact, the S_c^* represents the general topology condition for a co-operative transition to be possible and should be nearly the same for all glass forming liquids. Since the relaxation time τ or the viscosity of the glass forming liquid is inversely proportional to $\bar{W}(T)$,

$$\eta = A\exp\left(\Delta\mu S_c^*/KTS_c\right) \quad (11)$$

where A is a frequency factor term. Consequently, the temperature dependence of the viscosity in a glass forming liquid exponentially increases with $\Delta\mu/S_c$. Thus, the viscosity (or the relaxation) behaviour is substantially related to the co-operative transitions where the size of the co-operatively rearranging region is determined by the configurational entropy. According to either equilibrium [116] or quasi-equilibrium [123] theory, the configurational entropy S_c almost vanishes at T_g. From Equation 10, this means that a critical co-operative region size Z^* becomes infinite at T_g. In other words, a glass formation takes place homogeneously by the rearrangement of atoms or molecules throughout the entire body. In fact, this consideration shows good agreement with the usual glass transition observations [154]. Taking account of the facts that the glass transition occurs within a narrow temperature range and that the temperature dependence of the viscosity in a glass forming liquid is steeper than the prediction of the Fulcher equation [146], S_c will exponentally decrease to T_g on lowering the temperature from

T_m for a glass forming liquid. Consequently, it appears that S_c, instead of the term $\Delta\mu$, contributes predominantly to the viscosity in the temperature range between T_m and T_g. It is noteworthy that the computer calculation using hard spheres with dense random packing shows that the diffusion coefficient, D, and the fluidity, ϕ, would have virtually vanished well before the D.R.P. density is reached [155]. Since the configurational entropy in a glass forming liquid is frozen in at T_g, S_c is approximately constant below T_g. Thus this may result in playing a major role in determining the viscosity of a glass phase in the temperature range below T_g. Hence $\Delta\mu$ may substantially affect the stability of the amorphous phase.

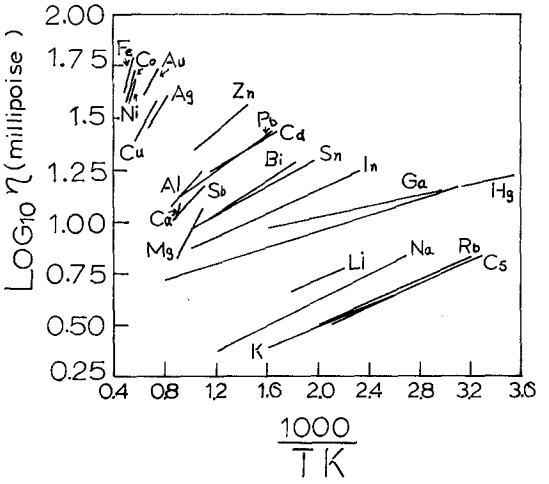

Figure 13 Experimental relation between viscosity and temperature for liquid metals [156].

With $T > T_m$ the temperature dependence of the viscosity in the liquid metal is generally expressed as

$$\log \eta = A/T + B \qquad (12)$$

where A and B are constants. Fig. 13 shows the viscosity–temperature relation for various liquid metals [156]. Since the temperature dependence of the configurational entropy for the liquid metal is approximately not as great as the difference between each metal [123, 133, 152], one can expect that the $\Delta\mu$ term is most important in determining the slope of the $\eta - 1/T$ relation above T_m.

Here, this $\Delta\mu$ may strictly relate not only to a cohesive energy, which includes repulsive and attractive interactions between constituent atoms, but also to the short range order (S.R.O.) structures in the glass forming liquid. In the foregoing view, the potential energy hindering the co-operative rearrangement for a constituent atom $\Delta\mu$, must be reflected in the formation and stability of the amorphous state. Recently, Chen systematically studied the glass transition temperature T_g in glassy alloys $(Pd_{1-x}M_x)_{0.835}\ Si_{0.165}$ for M = Fe, Ni, Co, Rh, Cu, Au and Ag, $(Pd_{1-x}N_x)_{1-x_p}\ P_{x_p}$ for N = Ni, Co and Fe, and $(Pt_{1-x}Ni_x)_{1-x_p}\ P_{1-x_p}$ [86]. He finds the evidence that the mixing enthalpy from a quasi-chemical calculation closely correlates to T_g. Therefore the ordering or clustering among metal constituent atoms may raise or lower T_g in the amorphous alloy, while the disturbance of the structure order lowers the melting temperature and enhances the stability of an amorphous state. Thus he concluded that the strong interaction between unlike atoms raises the glass temperature as well as causing the size effect. He further concluded that the strong interaction also causes a lowering of the melting temperature. However, some care must be taken in the case of the reduction of the melting point. The above conclusion could be valid only if the atomic interaction between unlike atoms was relatively weak, since if the interaction is relatively strong an intermetallic compound tends to appear and hence causes a rise in the liquidus curve in the phase diagram. Therefore, too strong an interaction between unlike atoms results in raising the melting temperature. Fig 14 shows the experimental results for the composition dependence versus the glass transition temperature T_g of $(Pd_{1-x}M_x)_{0.835}Si_{0.165}$

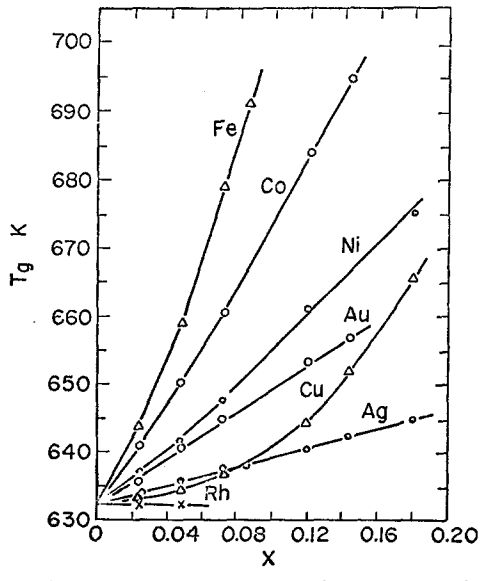

Figure 14 Composition dependence of the glass transition temperature T_g of $(Pd_{1-x}M_x)_{0.835}Si_{0.165}$ alloys. M = Cu, Ag, Ni, Co or Rh. Heating rate = 20 K min^{-1} [86].

alloys. In Fig. 14 T_g of the admixture with the transition and noble metals increase in roughly the order Fe, Co, Ni, Au, Cu and Ag for $x < 0.20$. This tendency of a rising T_g with the atoms in the above order cannot be explained except by the cohesive energy of the elements itself, the atomic size difference or the difference of the electronegativity, i.e. the atomic interaction (see Table III). It is, however, very interesting to compare Fig. 14 with Fig. 13. We can clearly recognize that the slope of the viscosity–temperature relation in liquid metals almost coincides with increasing T_g. Accordingly, since the slope is directly related to $\Delta\mu$ as mentioned above, it can be concluded that the potential energy hindering the co-operative rearrangement for a constituent atom, $\Delta\mu$, plays the most significant role in the stability and the formation of the amorphous state, though we need more systematic data to establish this fact. Thus functional dependence of $\Delta\mu$ of the liquid metal is roughly reflected in the dependence of T_g on M in the alloy $(Pd_{1-x}M_x)_{0.835}Si_{0.165}$ where M and Pd have nearly the same atomic radii. Above a critical concentration of the replaced element, the ordering or the clustering between unlike atoms will change over a short range, and hence the interaction among unlike atoms causes the change of the glass temperature T_g. This means that the mixing enthalpy would reflect in T_g.

5.4 Atomic interaction

The fifth column in Table III shows the electronegativity of the constituents. Generally the atomic interaction increases with the difference in electronegativity of the constituents and plays a major role in the tendency in forming an intermetallic compound [157]. In the case of the glass forming alloys in the transition metal and metalloid systems, they always exhibit, either in their molten or intermetallic compound state, negative heats of mixing when formed from the corresponding pure constituents [88, 120]. From the quasi-chemical analysis, this means that a strong interaction between unlike atoms in these alloys can exist, which in turn causes a high degree of short range order in either the molten or solid states. Indeed, it is revealed that a high degree of local order can exist in a molten [88, 120] and amorphous state [2, 7, 109]. The extent of the glass forming region in an amorphous alloy will be, in most cases, determined only by the metalloid content while the formation and the stability of an amorphous alloy will usually be enhanced by the metalloid content [17, 158]. Accordingly, these will definitely result from the strong interaction between the metal and the metalloid elements. Impurity effects on the glass forming thin films will now be discussed further. It has been reported that impurities remarkably enhance the formation and stability of an amorphous state [44, 135, 136, 159]. This impurity effect may possibly be explained by the following three reasons: (1) a strong atomic interaction between gaseous impurities and the bulk elements, (2) a reduction in the undercooling due to depression of T_m by impurity addition, and (3) a kinetic retardation of crystallization due to non-uniform atomic size.

The glass forming tendency may also be described by the reduced melting temperature τ_m given by

$$\tau_m = kT_m/h_v \qquad (13)$$

where T_m is the crystallization temperature and h_v is the heat of vaporization. Accordingly, τ_m measures the degree of diffusive atom mobility at T_m. The tendency for a glass to form increases with a decrease in T_m.

In conclusion, if we rank the factors important in the formation and stability of an amorphous material the most effective factor would be the potential energy barrier, $\Delta\mu$, for a constituent atom, the second the size difference effect, and the third the undercooling or cooling rate. Following this guide we might suggest other possible amorphous alloys from the periodic table given in Fig. 1 according to the following: (1) since there is a high possibility for the elements already produced as amorphous material in either the pure state or as an alloy, to form in the amorphous state, the combination of these elements, particularly using the method of SQ and EV, will be of prime consideration. (2) The possible alloy systems will be chosen for the presence of a eutectic composition in the phase diagram, i.e. this will give a measure of $\Delta\mu$. (3) The atomic radii of the elements in a possible amorphous system will be chosen so as to maximize their differences. It is interesting in Fig. 1 to note that few amorphous materials have been reported for the alkali metals (IA) and the divalent metals (IIA and IIB) in either pure or alloy state. This might result from their relatively low binding energy.

6. Structural model

The structure of an amorphous material has long been a mystery. Since Dixmier *et al.* first calculated the radial distribution function (R.D.F.) from X-ray intensity measurements in Ni–P amorphous alloys [2] many structural determinations have been performed by X-ray analysis. Recently, high resolution transmission electron microscopy, field ion microscopy, Mössbauer measurements and positron absorption measurement have also been used as aides in solving this problem. These studies revealed that amorphous structures were characterized by (1) a homogeneous structure [4, 7] rather than by internal boundaries separating small, well ordered regions and (2) a random atomic arrangement, where short range order is less than 15 ± 1 Å. Particularly, the X-ray diffraction intensity curve is characterized by a broad main peak which is sharper and more intense than that obtained from a liquid, and three or four very weak subpeaks [2, 7]. Moreover, it is often observed that the X-ray intensity curve of some amorphous alloys has a shoulder in the second peak [108].

To attempt to describe an amorphous structure, generally, three models have so far been prepared: a crystalline model [4, 160–162], a random layer lattice model [2] and a Bernal dense random packing model [4, 125, 133].

In the case of the crystalline model, one assumes a crystalline structure with a small size for the particular sample and calculates directly the interference function $i(k)$ with the Debye scattering equation [163]. Cargill calculated the interference function for fcc, hcp, and Ni_3P type crystals of small size in order to compare these to the experimental results obtained on Ni–P amorphous alloys. He found that these models did not completely fit the experimental observations even when account was taken for stacking faults and internal strains. However, an amorphous thin film, Ag–Cu, showed reasonable agreement with an fcc model, indicating that these films were microcrystalline [163]. Another crystalline model was the quasi-crystalline approach. This model starts with the atomic shell distances of the atoms and occupation numbers of a postulated crystalline structure, and then assumes a Gaussian distribution function for each shell in order to account for the thermal or disordering displacement around the center of the shell. Maitrepierre [7] calculated the radial distribution function (R.D.F.) to determine the structure of Ni–Pd–P and Fe–Pd–P amorphous alloys using this model. He concluded that the agreement on the Pd_3P (Pd-rich) structure with the experimental observations was satisfactory.

The random layer lattice model was used by Dixmier *et al.* to investigate Ni–P amorphous alloys [2]. The calculated interference function showed good agreement with their experimental results. Thus, they concluded that the structure of Ni–P amorphous alloys consisted of random packing of close-packed layers with finite dimensions. However, this model was criticized by Cargill [4a] who calculated the interference function taking into account in addition to the $(h\,k)$-type reflection considered by Dixmier *et al.*, the $(0\,0\,l)$ type reflection. He demonstrated that the spacing between layers r_1 necessary to reproduce the position of the first peak in the experimental interference function ($r_1 = 2.03$ Å) is much smaller than the atomic diameter of a nickel atom in crystalline nickel (2.49 Å). This implied that these close packed layers were not completely random as in carbon black where r_1 is greater than the spacing between atoms.

Finally, the Bernal dense random packing of hard spheres model (D.R.P.) has been used to investigate the amorphous structure. Bernal successfully simulated a simple monatomic liquid using dense random packing of hard spheres. This consisted of only five types of basic unit holes (Fig. 15) which were combined in a unlimited way. In Fig. 15 the holes a, b, c d and e make up 86.2, 5.9, 3.8, 0.5, and 3.7%, respectively, of the total holes present in the material in the D.R.P. model. The packing density ρ_p was determined as 0.6366 ± 0.0004, where ρ_p is expressed as

$$\rho_p = (4/3)\pi r^3/\bar{V} \qquad (14)$$

where r denotes the hard sphere radius and $\bar{V}$ the volume per sphere in the bulk structure.

Cohen and Turnbull proposed that the amorphous structure is truly metastable and that an ideal monatomic glass structure can be described by the D.R.P. model [123]. Cargill [4b] then calculated the pair distribution function $W(r) = \rho(r)/\rho_0$, where $\rho(r)$ is the radial distribution function and ρ_0 is the average density, using Finney's D.R.P. model, and showed that the $W(r)$ curve was in good agreement with the experimental curves obtained from Ni–P amorphous alloys when $2\sigma = 2.42$ Å where σ is the radius of the hard sphere (shown in Fig. 16). Polk [8] has pointed out that a value for 2σ of 2.48 Å gives, an even better fit to

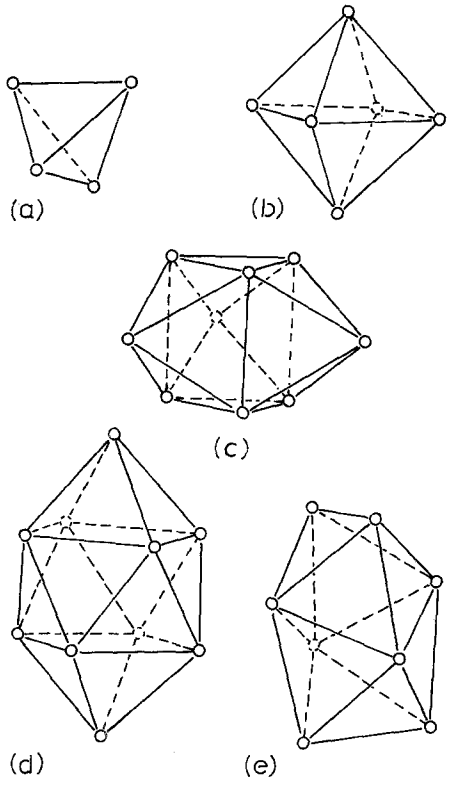

Figure 15 Basic constituent holes in Bernal DRP structure: (a) tetrahedron; (b) octahedron; (c) trigonal prism capped with three half-octahedra; (d) archimedian antiprism capped with two half-octahedra; (e) tetragonal dodecahedron [133].

the experimental curve. Moreover, he proposed that the metalloid atoms simply filled the larger holes between metal atoms in the Bernal D.R.P. structure. This is similar to the structure of soda-silica glasses where the soda ions fill the larger holes [164]. If the metalloid elements fill all of the larger holes in a D.R.P. structure, then the concentration of the metal elements would be 79%. This value is close to a eutectic composition for some binary alloys. However, Chen and Park criticized this model because the partial molar volume of Pd–Cu–Si metal glasses shows a linear dependence on composition [89]. Sadoc *et al.* [165] also disagreed with this model because of their results from computer calculations of the interference function $i(k)$, using the dense random packing of non-equal sized hard spheres model. It was found that the small spheres strongly affects the local arrangement of the large ones. Indeed in Ni–Pd–P amorphous alloys, the metal–metal nearest neighbour distances and metal–phosphorous distances are changed continuously with increasing phosphorous concentration [108]. These results can not be expected from the Polk model. It is quite probable, however, that a fraction of the holes are filled by metalloid atoms since the size of the metalloid atom is sufficiently small to fit into the holes when ionized. Indeed, it is thought that a metalloid element is often ionized in the amorphous state [5, 89, 93].

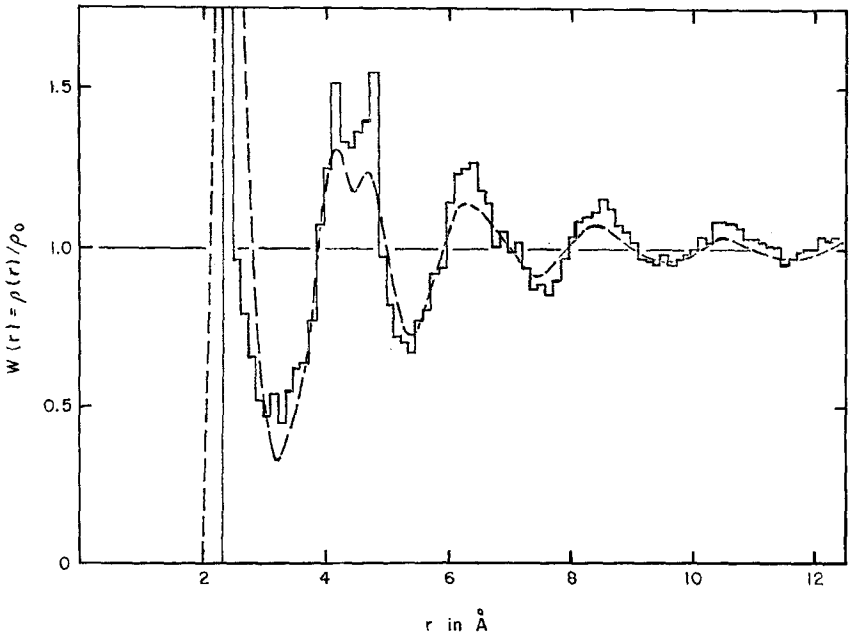

Figure 16 Comparison of $W(r) = \rho(r)/\rho_0$ for Finneys DRP with $2\sigma = 2.42$ Å (histogram) with $W(r)$ for Ni–P, 76 at.% Ni (broken curve) [4b].

It was shown that amorphous alloys, such as Au–Si [31] and Ni–Pt–P [5], exhibits neither the splitting of the second peak in the R.D.F. curve nor a shoulder at high K values of the second peak in diffraction patterns. Some X-ray data on amorphous alloys are summarized in Table IV. For comparison data on liquid Fe, Te-based glass, fused SiO_2, the D.R.P. model and the icosahedron structure also listed. The position r_1 of the first peak is usually taken as a measure of the interatomic distance in the amorphous state. The ratio r_2/r_1 is approximately 1.7 for most of the amorphous alloys except the Ni–Pt–P system. This is recognized as evidence that the amorphous structure of alloys is almost the same [7]. On the other hand, the ratio r_2/r_1 for Ni–Pt–P and Ag–Cu amorphous alloys is 1.86 and 1.75 respectively. These are close to the value for liquid metals (1.79). Moreover, the X-ray intensity curve of the liquid does not show a shoulder peak. Thus, amorphous alloys, Au–Si, Ag–Cu and Ni–Pt–P, were taken as the liquid metals having a high degree of disorder and whose constituents have a large atomic size difference [5, 17]. However, Chen and Park [89] criticized the size difference explanation because of the relative atomic sizes of Pd, P and Ni in Ni–Pd–P alloys which are similar to those of Pt, P and Ni in Pt–Ni–P alloys. They also suggested that the difference in the appearance of the R.D.F. curve is simply a reflection of differences in the short-range structure arrangements in the liquids. In fact, Dixmier and Duwez [108] have recently investigated the effect on the atomic distribution curve $W(r)$ of the phosphorous concentration in $(Pd_{50}Ni_{50})_{100-x}P_x$ metal glasses. Their result revealed that as the phosphorous content increases, the intensity of the first peak decreases, the first and second peaks broaden and the shoulder on the right side of the second peak begins to disappear. This phosphorous effect on the distribution function was also demonstrated by Sadoc *et al.* [165] using computer calculations of D.R.P. with two hard sphere sizes. Thus they concluded that a small phosphorous atom promotes special local arrangement of atoms, i.e. a short range order.

Although L in Table IV is not a good representation for amorphous alloys, L can, to a good approximation, be interpreted as an average microcrystalline dimension perpendicular to the diffracting plane [167]. L is less than 15 Å for most amorphous alloys. The co-ordination number CN was determined by the area under the first peak

TABLE IV Some X-ray data of amorphous alloys

Alloy	Composition range x(at.%)	γ_1(Å)	γ_2(Å)	γ_2/γ_1	L(Å)	CN	Reference
$Ag_{55}Cu_{45}$	–	2.83	4.95	1.75	–	13.0	[37]
$Cu_{35}Mg_{65}$	–	2.56	4.28	1.67	–	13.5	[37]
Fe	Pure	2.6	4.5	1.73	–	< 8	[6]
(liquid Fe)	Pure	2.51	4.5	1.79		8.4	[6, 161]
$Fe_{80}P_{13}C_7$	–	2.6	4.3	1.65	–	13.1	[6]
$Fe_{75}P_{16}C_{10}$	–	–	–		15.7	–	[5]
$Fe_{32}Pd_{48}P_{20}$	–	2.8	4.66	1.66		13.2 ± 0.5	[7]
$Fe_{44}Pd_{36}P_{20}$	–	2.76	4.65	1.68	13.6	14.6 ± 1.0	[7]
$Mn_{75}P_{15}C_{10}$	–	2.63	4.47	1.70	14.5	12.2	[166]
$Ni_{100-x}P_x$	26.2–18.6	2.57–2.54	4.29–4.43	1.67–1.74		12.97–13.02	[51]
$Ni_{32}Pd_{53}P_{15}$	–	2.78	4.60	1.65		12.7 ± 0.5	[7]
$Ni_{53}Pd_{27}P_{20}$	–	2.70	4.51	1.67	11.7	13.3 ± 0.5	[7]
$Ni_{41}Pd_{41}B_{18}$	–	–	–		12.4		[5]
$(Ni_xPt_{100-x})_{75}P_{25}$	20–60	2.85–2.77	5.35–5.10	1.88–1.84	17.6–10.1	11.4–11.8	[5]
$Pd_{80}Si_{20}$	–	2.75	4.70	1.71	14.6	11.6	[5, 3]
$Pd_{80}Si_{20}Ge_{10}$	–	–	–	–	15.8	–	[5]
$Te_{100-x}Ga_x$	10–30	2.65–2.70	4.05–4.10	–	–	1.3–2.2	[96–98]
$Te_{100-x}Ge_x$	10–25	2.60–2.70	4.00–4.05	–	–	1.3–1.6	[96–98]
$Te_{100-x}In_x$	10–30	2.70–2.80	4.15–4.25	–	–	2.0–2.3	[96–98]
(fused SiO_2)	–	–	–	–	10.0	–	[5]
(icosahedron)	–	–	–	–	–	12	[133]
(D.R.P.)	–	–	–	–	–	3–11	[133]

Notes: γ_1 and γ_2 denote first and second peaks position of a reduced radial distribution function respectively. L = the size parameter which was calculated by using Scherrer formula, i.e. $L = 51\lambda/(\Delta 2\theta)\cos\theta$ where $(\Delta 2\theta)$ is the width at half-maximum height of a particular peak of the intensity curve. CN is a co-ordination number, D.R.P. is a Bernal dense random mixing of hard spheres model.

of a R.D.F. curve using

$$CN = 4\pi r^2 \rho(r) \mathrm{d}r. \qquad (15)$$

The CN of a noncrystalline solid is roughly 12 ± 1 which is larger than that of liquid metals.

7. Conclusions

The configurational entropy is a more suitable parameter than any other to consider the formation and stability of amorphous phases. In particular, the potential barrier for a constituent atom, $\Delta\mu$, plays the most significant role in the stability and the formation of the amorphous state; a large $\Delta\mu$ increases the stability and the tendency of formation for the amorphous state. This $\Delta\mu$ may strictly relate not only to a cohesive energy, which includes repulsive and attractive interactions between constituent atoms, but also to the short range order structure in the glass forming liquid or amorphous state. However, we need more data to establish these conclusions.

Acknowledgements

The author would like to warmly thank Professor D. R. Gaskell, Dr L. A. Davis and the staff of the Strength Physics Department of the Materials Research Center for their valuable comments and advice. I am also grateful to Professor R. Maddin for his continuing advice and encouragement throughout my graduate education in the University of Pennsylvania. This work was supported by the National Science Foundation.

References

1. H. RICHTER, *Z. Physik.* **44** (1944) 406.
2. J. DIXMIER, K. DOI and A. GUINIER, in "Physics of Noncrystalline Solids", edited by J. A. Prins (North Holland, Amsterdam, 1965) p. 67.
3. R. C. CREWDSON, Ph.D. Thesis, California Institute of Technology, Pasadena, California (1966).
4. G. S. CARGILL III, (a) *J. Appl. Phys.* **41** (1970) 12; (b) *ibid* **41** (1970) 2248.
5. A. K. SINHA and P. DUWEZ, *J. Phys. Chem. Solids* **32** (1971) 267.
6. S. C. H. LIN and P. DUWEZ, *Phys. Stat. Sol.* **34** (1969) 469.
7. P. L. MAITREPIERRE, *J. Appl. Phys.* **40** (1969) 4826.
8. D. E. POLK, (a) *Scripta Met.* **4** (1970) 117; (b) *Acta Met.* **20** (1972) 485.
9. R. BRILL, *Z. Kristallogr.* **75** (1930) 217.
10. A. BRENNER and G. RIDDELL, *J. Res. Nat. Bur. Stand.* **39** (1947) 385.
11. A. BRENNER, D. E. COUCH and C. K. WILLIAMS, *ibid* **44** (1950) 109.
12. A. W. GOLDENSTEIN, W. ROSTOKER and F. SCHOSSBERGER, *J. Electrochem. Soc.* **104** (1957) 104.
13. W. BUCKEL, *Z. Phys.* **138** (1954) 136.
14. W. RUHL, *ibid* **138** (1954) 121.
15. W. BUCKEL and R. HILSON, *ibid* **131** (1952) 420.
16. W. KLEMENT, JUN., R. H. WILLENS and P. DUWEZ, *Nature* **187** (1960) 869.
17. B. C. GIESSEN and C. N. J. WAGNER, in "Physics and Chemistry of Liquid Metals", edited by S. Z. Beer (Marcel Dekker, New York, 1972) p. 633.
18. G. V. GOKULARATHNAM, *J. Mater. Sci.* **9** (1974) 673.
19. P. DUWEZ, *Trans. Met. Soc. AIME* **60** (1967) 605.
20. P. DUWEZ and R. H. WILLENS, *ibid* **227** (1963) 362.
21. R. H. WILLENS and E. BUCHLER, *ibid* **236** (1966) 171.
22. P. PIETROKOWSKY, *Rev. Sci. Instrum.* **34** (1963) 445.
23. P. RAMACHANDRARAO, D. BANERJEE and T. R. ANANTHARAMAN, *Met. Trans.* **1** (1970) 2655.
24. M. MOSS, D. L. SMITH and R. A. LEFEVER, *Appl. Phys. Letters* **5** (1964) 120.
25. K. YAMAUCHI and Y. NAKAGAWA, *Jap. J. Appl. Phys.* **10** (1971) 1730.
26. R. ROBERGE and H. HERMAN, *Mat. Sci. & Eng.* **3** (1968) 62.
27. R. POND, JUN. and R. MADDIN, *Trans. Met. Soc. AIME.* **245** (1969) 2475.
28. H. S. CHEN and C. E. MILLER, *Rev. Sci. Instrum.* **41** (1970) 1237.
29. J. J. GILMAN, Allied Chemical Mat. Res. Rep. November 9 (1973).
30. H. S. CHEN and D. TURNBULL, *J. Appl. Phys.* **38** (1967) 3646.
31. J. DIXMIER and A. GUINIER, *Mem. Sci. Rev. Met.* **64** (1967) 53.
32. P. PREDECKI, B. C. GIESSEN and N. J. GRANT, *Trans. Met. Soc. AIME.* **233** (1965) 1438.
33. B. C. GIESSEN, *Z. Metallk.* **59** (1968) 805.
34. T. R. ANANTHARAMAN, H. L. LUO and W. KLEMENT, JUN., *Trans. Met. Soc. AIME.* **233** (1965) 2014.
35. H. S. CHEN and D. TURNBULL, *Appl. Phys. Letters* **10** (1967) 284.
36. S. MADER, H. WIDMER, F. M. D'HEURLE and A. S. NOWICK, *ibid* **3** (1963) 201.
37. C. N. J. WAGNER, *J. Vac. Sci. Techn.* **6** (1969) 650.
38. W. C. KOK, *Phil. Mag.* **30** (1974) 351.
39. H. A. DAVIS and J. B. HULL, (a) *Script. Met.* **6** (1972) 241; (b) *J. Mater. Sci.* **9** (1974) 707.
40. U. KÖSTER, *Acta. Met.* **20** (1972) 1361.
41. H. A. DAVIS and J. B. HULL, *Script. Met.* **7** (1973) 637.
42. R. HILSCH, in "Non-crystalline Solids", edited by V. D. Frechette (Wiley, New York, 1960) Ch. 15.
43. F. GALASSO, R. VASLET and J. PINTO, *Appl. Phys. Letters* **8** (1966) 331.
44. J. C. SUITS, *Phys. Rev.* **131** (1963) 588.

45. C. W. B. GRIGSON and D. B. DOVE, *J. Vac. Sci. Tech.* 3 (1966) 120.
46. J. R. BOSNELL, *Thin Solid Films* 3 (1969) 233.
47. H. A. DAVIS, J. AUCOTE and J. B. HULL, *Nature* **246** (1973) 13.
48. S. FUJIME, *Jap. J. Appl. Phys.* 6 (1967) 305.
49. K. L. CHOPRA, M. R. RANDLETT and R. H. DUFF, *Appl. Phys. Letters* 9 (1966) 402.
50. T. E. HUTCHINSON, (a) *J. Appl. Phys.* **36** (1965) 270; (b) *Appl. Phys. Letters* 3 (1963) 51.
51. P. N. DENBIGH and R. B. MARCUS, *J. Appl. Phys.* **37** (1966) 4325.
52. N. A. GORYUNOVA, E. F. GRASS, L. B. ZLATKIN and E. K. IVANOV, *J. Non-Cryst. Solids* 4 (1970) 57.
53. S. MADER and A. S. NOWICK, *Appl. Phys. Letters* 7 (1965) 57.
54. A. BRENNER, "Electrodeposition of Alloys, Principles and Practices" (Academic Press, New York, 1963) pp. 187, 611.
55. D. PAN and D. TURNBULL, *J. Appl. Phys.* **45** (1974) 1406.
56. R. RAY, B. C. GIESSEN and N. J. GRANT, *Script. Met.* 2 (1968) 357.
57. A. REVCOLEVSCHI and N. J. GRANT, *Met. Trans.* 3 (1972) 1545.
58. P. H. SHINGU, K. KOBAYASHI, K. SHIMOMURA and R. OZAKI, *Script. Met.* 8 (1973) 1317.
59. R. J. FORT and W. R. MOORE, *Trans. Faraday Soc.* **62** (1966) 1112.
60. P. DUWEZ and S. C. H. LIN, *J. Appl. Phys.* **38** (1967) 4096.
61. D. E. POLK and H. S. CHEN, *J. Non-Cryst. Solids* **15** (1974) 165.
62. A. K. SINHA, *J. Appl. Phys.* **42** (1971) 338.
63. M. BARMATZ and H. S. CHEN, *Phys. Rev. B.* **9** (1974) 4073.
64. D. E. POLK and C. A. PAMPILLO, *Script. Met.* 7 (1973) 1161.
65. H. S. CHEN and D. POLK, *J. Non-Cryst. Solids* **15** (1974) 174.
66. T. MASUMOTO, private communication.
67. R. HASEGAWA and J. A. DERMON, *Phys. Letters* **42A** (1973) 407.
68. P. CHARDHARI, J. J. CUOMO and R. J. GAMBINO, *Appl. Phys. Letters* **22** (1973) 337.
69. S. R. HERD and P. CHANDHARI, *Phys. Stat. Sol. (a)* **18** (1973) 603.
70. J. OREHOTSLCY and K. SCHRÖDER, *J. Appl. Phys.* **43** (1972) 2413.
71. R. W. VASS, M. A. MEININGER and R. M. ANDERSON, *ibid* **45** (1974) 843.
72. W. L. JOHNSON, S. J. POON and P. DUWEZ, *Phys. Rev. B* **11** (1975) 150.
73. R. P. FERRIER and D. J. HERRELL, *J. Non-Cryst. Solids* 2 (1970) 278.
74. H. H. HESTER and W. D. KINGERY, in "International Conference on Glasses, Brussels" (1963) p. 106.
75. A. F. POLESYA and V. N. GUDZENKO, *Izvest. Akad. Nauk SSSR, Neorg, Materialy* **10** (1974) 1011.
76. R. HASEGAWA, *Phys. Rev. B* 3 (1971) 1631.
77. R. RUHL, B. C. GIESSEN, M. COHEN and N. J. GRANT, *Acta. Met.* **15** (1967) 1693.
78. V. K. C. LIANG and C. C. TSUEI, *Phys. Rev. B* 7 (1973) 3215.
79. P. RAMACHANDRARAO, P. K. GARG and T. R. ANANTHARAMAN, *Ind. J. Tech.* 8 (1970) 263.
80. B. C. GIESSEN, "Proceedings of the 12th Army Materials Research Conference" (Syracuse University Press, Syracuse, New York, 1966) p. 273.
81. P. DUWEZ, R. H. WILLENS and R. C. CREWDSON, *J. Appl. Phys.* **36** (1965) 2267.
82. R. HASEGAWA and C. C. TSUEI, *Phys. Rev. B* 2 (1970) 1631.
83. C. C. TSUEI and P. DUWEZ, *J. Appl. Phys.* 37 (1966) 435.
84. R. HASEGAWA and C. C. TSUEI, *Calif. Inst. Tech. Rep.* CALT-221-90 (1970).
85. R. HASEGAWA, *J. Phys. Chem. Solids* **32** (1971) 2487.
86. H. S. CHEN, *Acta. Met.* **22** (1974) 1505.
87. R. HASEGAWA, *J. Appl. Phys.* **43** (1972) 1231.
88. H. S. CHEN and D. TURNBULL, *Acta. Met.* 17 (1969) 1021.
89. H. S. CHEN and B. K. PARK, *ibid* **21** (1973) 395.
90. N. I. MARZWELL, *Calif. Tech. Rep.,* CALT-822-53 and 55 (1973).
91. B. Y. BOUCHER, *ibid* CALT-822-35 (1971).
92. R. C. CREWDSON, *ibid* CALT-221-20, 21 (1966).
93. A. K. SINHA, *Phys. Rev. B.* **1** (1970) 4541.
94. A. K. SINHA, *Calf. Tech. Rep.* CALT-822-31 (1971).
95. R. HASEGAWA, *Phys. Letters* 38A (1972) 5.
96. R. H. WILLENS, *J. Appl. Phys.* **33** (1962) 3269.
97. H. L. LUO and P. DUWEZ, *Appl. Phys. Letters* 2 (1963) 21.
98. H. L. LUO, *Calif. Tech. Rep.,* No. 22 (1964).
99. M. CUTLER and C. E. MALLON, *Phys. Rev.* **114** (1966) 642.
100. R. P. FERRIER, J. M. PARDO and M. R. ANSEAU, *J. Non-Cryst. Solids* **8–10** (1972) 798.
101. H. L. LUO, *Abst. Bull. IMD-AIME.* 2 (1) (1967) 44.
102. M. SEGNINI, B. C. GIESSEN and R. RAY, unpublished.
103. R. HASEGAWA, *Phys. Rev. Letters* **28** (1972) 1376.
104. S. TAKAYAMA, Ph.D. Thesis. University of Pennsylvania (1974).
105. G. FALKENHAGEN and W. HOFMANN, *Z. Met.* **43** (1952) 69.
106. N. J. GRANT, *Fizika 2. Suppl.* 2 (1970) 16. 1
107. P. DUWEZ, R. H. WILLIAMS and K. KLEMENT, JUN., *J. Appl. Phys.* **31** (1960) 36.
108. J. DIXMIER and P. DUWEZ, *J. Appl. Phys.* **44** (1973) 1189.
109. A. HOWIE, O. KRIVANEK and M. L. RUDEE, Proceedings of the Fifth European Congress on Electron Microscopy (Institute of Physics, London, 1972) p. 450.
110. J. M. SCHULTZ, "Principles of Polymer System" Polymer Materials Science (Prentice-Hall, New Jersey, 1974).
111. S. C. H. LIN, *J. Appl. Phys.* **40** (1969) 2175.
112. C. C. TSUEI, G. LONGWORTH and S. C. H. LIN, *Phys. Rev.* **170** (1968) 603.

113. D. TURNBULL and M. COHEN, *J. Chem. Phys.* **34** (1961) 120.
114. J. A. PRINS, in "Physics of Non-Crystalline Solid", edited by J. A. Prins (North-Holland, Amsterdam, 1965) p. 2.
115. H. S. CHEN, J. T. KRAUSE and E. A. SIGETY, *J. Non-Cryst. Solids* **13** (1973/74) 321.
116. J. H. GIBBS and E. A. DIMARZIO, *J. Chem. Phys.* **28** (1958) 373.
117. G. ADAM and J. H. GIBBS, *ibid* **43** (1965) 139.
118. R. J. GREET and D. TURNBULL, *ibid* **47** (1967) 2185.
119. W. KAUZMANN, *Chem. Revs.* **43** (1948) 219.
120. H. S. CHEN and D. TURNBULL, *J. Chem. Phys.* **48** (1968) 2560.
121. B. G. BAGLEY, H. S. CHEN and D. TURNBULL, *Mat. Res. Bull.* **3** (1968) 159.
122. D. TURNBULL, in ASM Seminar on Solidification, Cleveland (1969).
123. M. H. COHEN and D. TURNBULL, *Nature* **203** (1964) 964.
124. D. WEAIRE, M. F. ASHBY, L. LOGAN and M. J. WEINS, *Acta. Met.* **19** (1971) 779.
125. J. L. FINNEY, *Proc. Roy. Soc.* **319A** (1970) 479, *ibid* **319A** (1970) 495.
126. M. H. COHEN and D. TURNBULL, *J. Chem. Phys.* **31** (1959) 1164.
127. D. R. UHLMANN, *J. Non-Cryst. Solids* 7 (1972) 337.
128. H. A. DAVIES, J. AUCOTE and J. B. HULL, *Script. Met.* 8 (1974) 1179.
129. P. H. SHINGU and R. OZAKI, *Met. Trans.* **6A** (1975) 33.
130. T. R. ANANTHARAMAN, H. L. LUO and W. KLEMENT, JUN., *Trans. Met. Soc.* **233** (1965) 233.
131. M. HANSEN and K. ANDERKO, in "Constitution of Binary Alloys" (McGraw-Hill, New York, 1958) p. 206.
132. S. MADER, A. S. NOWICK and H. WIDMER, *Acta. Met.* **15** (1967) 203.
133. J. D. BERNAL, (a) *Nature* **185** (1960); (b) *Proc. Roy. Soc.* **280A** (1964) 299.
134. C. H. BENNETT, *J. Appl. Phys.* **43** (1972) 2727.
135. K. L. CHOPRA, "Thin Film Phenomena" McGraw-Hill, New York, 1969) p. 195.
136. K. H. BEHRNDT, *J. Vac. Sci. Tech.* 7 (1970) 385.
137. A. S. NOWICK and S. MADER, *I.B.M., J. Res. & Dev.* 9 (1965) 358.
138. S. MADER, *J. Vac. Sci. Tech.* **2** (1965) 35.
139. B. J. ALDER, *J. Chem. Phys.* **40** (1964) 2724.
140. H. S. CHEN, Proc. Phase Transitions, Pennsylvania State University, University Park, Pa. (1973) pp. 271–276.
141. G. A. MANSOURI, N. F. CARHAHAN, K. E. STARLING and T. W. LOLAND, JUN., *J. Chem. Phys.* **54** (1971) 1523.
142. A. K. DOOLITTLE, *J. Appl. Phys.* **22** (1951) 1471.
143. M. F. WILLIAMS, R. F. LANDEL and J. D. FERRY, *J. Amer. Chem. Soc.* **77** (1955) 3701.
144. R. E. HOFFMANN, *J. Chem. Phys.* **20** (1952) 1567.
145. N. H. NACHTRIEB and J. PETIT, *J. Chem. Phys.* **24** (1956) 746.
146. D. E. POLK and D. TURNBULL, *Acta. Met.* **20** (1972) 493.
147. W. T. LAUGHLIN and D. R. UHLMANN, *Bull. Amer. Aram. Soc.* **47** (1968) 402.
148. H. J. FISHER and A. PHILLIPS, *J. Met., Trans. AIME.* **6** (1954) 1060.
149. R. N. BARFIELD and J. A. KITCHENER, *J. Iron Steel Inst.* **180** (1955) 324.
150. A. A. ROMANOV and V. G. KOOHEGAROV, *Fiz. Metal. Metalloid* **17** (1964) 300.
151. R. A. SWALLIN, in "Thermodynamic of Solids" (Wiley, New York, 1962) Ch. 9.
152. D. TURNBULL and M. H. COHEN, *J. Chem. Phys.* **29** (1958) 1049.
153. J. H. HILDEBRAND, *ibid* **15** (1947) 225.
154. D. TURNBULL, *Contemp. Phys.* **10** (1969) 473.
155. B. J. ALDER, D. M. GASS and T. E. WAINWRIGHT, *J. Chem. Phys.* **53** (1970) 3813.
156. S. W. STRAUSS, *Nucl. Sci. Eng.* **12** (1962) 436.
157. C. KITTEL, in "Introduction to Solid State Physics", 2nd Edn (Wiley, New York, 1956).
158. P. DUWEZ, *Fizika 2 Suppl.* **2** (1970) 1. 1.
159. M. R. BENNETT and J. D. WRIGHT, *Phys. Stat. Sol.* **13A** (1972) 135.
160. R. KAPLOW, S. L. STRONG and B. L. AVERBACH, *Phys. Rev.* **138** (1965) A1336.
161. H. RUPPERSBERG and H. J. SEEMANN, *Z. Naturforsch* **21a** (1966) 820.
162. R. HOSEMAN and S. N. BAGCHI, in "Direct Analysis of Diffraction by Matter" (North-Holland, Amsterdam, 1962).
163. C. N. J. WAGNER, T. B. LIGHT, N. C. HALDER and W. E. LUKENS, *J. Appl. Phys.* **39** (1968) 3690.
164. L. W. TILTON, *J. Res. Nat. Bur. Stand.* **59** (1957) 139.
165. J. A. SADOC, J. DIXMIER and A. GUINIER, *J. Non-Cryst. Solids* **12** (1973) 46.
166. A. K. SINHA and P. DUWEZ, *Cal. Tech. Rep.* CALT-822-21 (1971).
167. B. E. WARREN, "X-ray Diffraction" (Addison-Wesley, Mass., 1969) pp. 120, 255.

Received 21 January and accepted 8 May 1975.